THESIS

CELLULOSE NANOCRYSTALS EXTRACTED FROM HEMP AGRO-WASTE AS A POTENTIAL COATING FOR TITANIUM MEDICAL DEVICES

Submitted by

Jesse Andrew Heacock

School of Biomedical Engineering

In partial fulfillment of the requirements

For the Degree of Master of Science

Colorado State University

Fort Collins, Colorado

Fall 2024

Master's Committee:

Advisor: Yan Vivian Li

Matt Kipper
James Liu

ABSTRACT

CELLULOSE NANOCRYSTALS EXTRACTED FROM HEMP AGRO-WASTE AS A POTENTIAL COATING FOR TITANIUM MEDICAL DEVICES

Increases in biowaste worldwide have created a unique opportunity to extract natural polymers for a variety of uses. Over the last few decades, hemp has increased in popularity as a desirable industrial agricultural plant. Increases in hemp production for commercial product use have increased the amount of hemp agro waste (HAW). This agro-waste is a potentially great source for extraction of the natural polymer cellulose and the creation of a circular economy. Cellulose can be found ubiquitously in plants and has gained great interest as an alternative to synthetic polymers. In this work, cellulose nanocrystals (CNCs) were extracted from HAW using a one-step ammonium persulfate (APS) oxidation method. APS oxidation was used due to its reduction in hazardous wastes, making it a more environmentally friendly method for CNC extraction compared to other chemical methods. HAW, specifically the woody core of hemp known as hurd, underwent CNC extraction and the properties of the final product were analyzed. Depending on the initial source and method of extraction, CNCs properties have been shown to vary, creating a potential for selectivity when applying CNCs for different uses. It was found that changes in reaction time directly impact CNCs size, surface properties, final product mass, and hydrophilicity. Of note, as reaction time increased from 8 hours to 48 hours, the size of the nanocrystals significantly decreased in length and width. While other properties, such as mechanical strength, morphology, surface charge, and cytotoxicity, underwent no statistically significant changes due to increases in reaction time. The results suggest that HAW is a good

source for CNC extraction and that changes in APS oxidation can allow for selective tuning of some CNC properties.

ACKNOWLEDGMENTS

This work was supported by the Colorado Agricultural Experimental Station Grant (COL00408) and the student research grant funded by the American Association of Chemists and Colorists. The authors would like to acknowledge the ARC Materials and Molecular Analysis (MMA) at Colorado State University for providing equipment for material characterizations.

The author would like to specifically thank the following people: Dr. Yan Vivian Li for her support and guidance throughout my research, Dr. Ketul Popat for believing in my abilities; Dr. Bryan Newell for support on the XRD analysis; Dr. Yu Sun for all his time and support learning the equipment in our lab; Morgan Davis for spending months with me working on the contact angle Theta Flex. The author also wishes to thank all his friends, new and old, for their encouragement and support during my time at CSU.

DEDICATION

To my Partner, Oksana Bennion

Your love, support, and compassion made this journey possible!

TABLE OF CONTENTS

ABSTRACT 1
ACKNOWLEDGMENTS 3
DEDICATION 4
LIST OF TABLES 7
LIST OF FIGURES 8
CHAPTER 1: INTRODUCTION 10
CHAPTER 2: MECHANICAL AND MORPHOLOGICAL PROPERTIES OF CELLULOSE NANOCRYSTALS EXTRACTED FROM INDUSTRIAL HEMP AGRO-WASTE 13
2.1 Summary 13
2.2. Introduction 15
2.3. Materials and Experiments 18
2.3.1 Materials 18
2.3.2 Synthesis of CNC Nanoparticles 19
2.3.3 Chemical Analysis 20
2.3.4 Crystallinity Measurement 21
2.3.5 Size and Morphological Characterization 21
2.3.6 Mechanical Analysis 22
2.4 Results and Discussion 23
2.4.1 Chemical and Elemental Composition 25
2.4.2 Size and Morphology Analysis 29
2.4.3 Mechanical property analysis 33
2.5 Conclusion 37
REFERENCES 40
CHAPTER 3: EFFECTS OF AMMONIUM PERSULFATE OXIDATION REACTION TIME ON PERFORMANCE PROPERTIES OF CELLULOSE NANOCRYSTALS DERIVED FROM HEMP AGRO-WASTE 45
3.1 Summary 45
3.2 Introduction 46
3.3. Materials and Experiments 48
3.3.1 Materials 48

3.3.2 Synthesis of CNC Nanoparticles 48
3.3.3 CNC percent yield 49
3.3.4 Fourier transform infrared spectroscopy (FTIR) 50
3.3.5 Dynamic Light Scattering (DLS) and Zeta Potential 50
3.3.6 Atomic Force Spectroscopy (AFM) 51
3.3.7 AFM – Force Distance Spectroscopy (FDS) 51
3.3.8 Wettability 52
3.3.9 Cytotoxicity 52
3.3.10 Statistical Analysis 53
3.4 Results and discussion 53
3.4.1 CNC dispersion and colloidal stability 53
3.4.2 Size and morphology 55
3.4.3 FTIR analysis 60
3.4.4 CNC mechanical properties 61
3.4.5 Surface wettability 63
3.4.6 CNC cytotoxicity 66
3.5. Conclusion 67
REFERENCES 69
CHAPTER 4: CONCLUSIONS AND FUTURE WORK 73
4.1 Conclusions 73
4.2 Future Work 74
4.2.1 CNC binding to Titanium 74
4.2.2 CNC surface modification 75
4.2.3 Electrospinning CNCs 75
REFERENCES 76

LIST OF TABLES

Table 3.1: CNC Size and Surface Properties……..……42
Table 3.2: CNC Mechanical Properties……..……46

LIST OF FIGURES

Figure 2.1:Synthesis of cellulose nanocrystals from hemp agro-waste: (a) Major synthesis steps and (b) Purification process. 19
Figure 2.2: Zeta potential for colloidally stable CNC particles in water; (a) Purified CNC solution, (b) Graphic of purified CNCs in water, and (c) Distribution of zeta potential for CNC. 24
Figure 2.3: Chemical and Elemental analysis of CNCs: (a) FTIR spectra, (b) SEM-EDS of UP-CNC, and (c) SEM-EDS of P-CNC. 27
Figure 2.4: XRD graphs for HAW, UP-CNC, and P-CNC samples. 28
Figure 2.5: DLS size distribution of CNC were analyzed using multiple runs on each sample. Measurements were performed on two samples and the size distributions are shown: (a) P-CNC size distribution and (b) UP-CNC size distribution. Visual representations of the individual solutions shown: (c) P-CNC graphic including CNC Zeta Potential and (d) UP-CNC graphic... 30
Figure 2.6: AFM images with size distributions of CNCs derived from hemp waste. (a) Topology image taken from UP-CNC sample, (b) Force image taken from P-CNC sample, (c) Topology for field of CNCs with height profile graphs (i, ii, and iii), and (d) Length and width size profile histograms of UP-CNC samples (i) and P-CNC samples (ii). 32
Figure 2.7: Force/distance mechanical measurement and measured mechanical characteristics of CNC: (a) AFM cantilever approaching CNC, (b) AFM cantilever upward deflection during indentation, (c) AFM Cantilever downward deflection during retraction, (d) Force/distance spectroscopy curve measurement, (e) Maximum applied load (nN) of cantilever applied to CNC, (f) Adhesion energy (aJ) between CNC and cantilever, and (g) Young's modulus (GPa) of CNC. 34
Figure 3.1: 4% w/v CNC aqueous dispersions (top row), DLS hydrodynamic radius (h), and Zeta potential of 8-CNC (a), 12-CNC (b), 16-CNC (c), 20-CNC (d), 24-CNC (e), 36-CNC (f), and 48-CNC (g)..... 54
Figure 3.2: Dried CNC samples: 8-CNC (a), 12-CNC (b), 16-CNC (c), 20-CNC (d), 24-CNC (e), 36-CNC (f), and 48-CNC (g)..... 56
Figure 3.3: AFM images (first and second rows), length distribution (h), and width distribution (i) of 8-CNC (a), 12-CNC (b), 16-CNC (c), 20-CNC (d), 24-CNC (e), 36-CNC (f), and 48-CNC (g). 58
Figure 3.4: FTIR spectra of hemp extracted CNCs at different reation times: 8-CNC, 12-CNC, 16-CNC, 20-CNC, 24-CNC, 36-CNC, and 48-CNC. 60
Figure 3.5: AFM-FDS adhesion energy (a) and Young's modulus (b) of 8CNC, 24-CNC, and 48-CNC. 62
Figure 3.6: Titanium coated with CNCs (row 1 and 2) and surface wettability (i) of 8-CNC (a), 12-CNC (b), 16-CNC (c), 20-CNC (d), 24-CNC (e), 36-CNC (f), 48-CNC (g), and pure Titanium (h). Statistical significances (p-value) were represented as * $p \leq 0.05$ and *** $p \leq 0.0001$. 64

Figure 3.7: Cytotoxicity studies of CNCs against ADSCs. The values are represented as absorbance values at 490 and 680 nm. Control and Triton represent spontaneous and maximum LDH release values. Statistical significances (p-value) were represented as ** $p \leq 0.001$. 67

CHAPTER 1: INTRODUCTION

With the demand for sustainable industrial crops increasing globally, hemp is emerging as a good alternative to other crops such as cotton. As hemp production increases, so does the need for sustainable means for disposing of the hemp biowaste. By repurposing and using this biowaste as a source to extract cellulose, value can be added to the industrial crop industry, as well as other manufacturing industries, by creating a circular economy. Cellulose, being ubiquitous in plants, is a sustainable and biodegradable natural polymer. The amount of cellulose available varies between plant species. Hemp biowaste, specifically hemp hurd, has a relatively large percentage of cellulose, 40 – 48%, making it a great source material for cellulose extraction. In order to extract cellulose, all other non-cellulosic material must be removed. The removal of non-cellulosic material can be done mechanically, chemically, or using a mechanical/chemical combination. Chemical methods for removing non-cellulosic material can aid in breaking large cellulose fibers into cellulose nanocrystals (CNCs). These methods of CNC extraction, generally, require harsh chemical treatment and the use of these chemicals can produce large amounts of hazardous waste. Ammonium persulfate oxidation (APS), however, has emerged in the last decade as a potential environmentally friendly alternative for the extraction of CNCs. APS is a one-step method for CNC extraction that reduces hazardous waste production. Furthermore, APS waste materials can be recovered post extraction, significantly reducing waste. Thus, APS oxidation in tandem with hemp biowaste, offers great potential for the extraction of CNCs in an eco-friendly manner to increase cellulose production.

CNCs have natural properties, such as biodegradability and biocompatibility, that make it an ideal material to replace synthetic polymers that are otherwise nonbiodegradable. The natural

properties of CNCs make this material versatile due to its tunability and usable for many different applications. These nanoparticles have been extracted from many different plant materials, as well as different types of waste materials such as denim and cardboard. Their properties have been documented and it has been shown that CNCs from different sources can vary in size, morphology, thermal, surface, and mechanical properties. To date the use of APS to extract CNCs from hemp biowaste has not been researched. Thus, raising the question, can CNCs be extracted from hemp hurd using APS and what properties do the resulting nanoparticles have. It was hypothesized that CNCs can be extracted from hurd using APS. The primary objective in chapter 2 was to analyze the nanoparticles material properties, with a particular interest in the mechanical properties of individual CNCs. The secondary objective was to determine if CNCs in various states, such as agglomerated in large groups or separated into individual particles, would cause differences in the measured Young's modulus.

One quality of CNCs that has gained a lot of attention over the years is their tunability. These nanoparticles can have their surface chemistry and charge altered by adding or removing different functional groups. Not only functional groups, but proteins, polymers, and drugs can be added to the surface of the nanoparticles. By changing the method of CNC extraction, the final product can be altered. This brought the question to mind, how does changing specific parameters using APS extraction impact CNCs from hemp hurd? It was hypothesized that CNC properties will have noticeable differences when changing the reaction time, holding all other reaction parameters constant. In chapter 3, the primary objective was to analyze material property changes to CNCs by varying reaction time from 8 to 48 hours. Chemical, morphological, and surface properties were all analyzed. Of particular interest was how reaction time impacted mechanical properties and cytocompatibility. Furthermore, hydrophilicity of these

particles were analyzed to determine changes, if any, that could be seen when using the nanoparticles to coat the surface of Titanium.

CNCs were successfully extracted from hemp biowaste using a modified APS oxidation method. CNCs were found to be uniform and reproducible between batches extracted using the same method (reaction time). However, these nanocrystals were found to have slight variations in properties between groups depending on changes in the method of extraction.

The research presented in this master's thesis is one of few studies focused on the extraction of cellulose from hemp biowaste using APS oxidation and the only study currently found that investigates the mechanical properties of individual CNCs from hemp biowaste using atomic force microscopy-force/distance spectroscopy. This investigation addresses the hypothesis that the Young's modulus of CNCs vary depending on source material/method of extraction. The studies purpose is to quantitatively determine the characteristics of CNCs from hemp biowaste. The findings of this series of experiments in this document offer insights into the differences in CNCs based on changes to extraction methods and how those differences can be utilized to specifically tune CNCs for different desirable applications.

CHAPTER 2: MECHANICAL AND MORPHOLOGICAL PROPERTIES OF CELLULOSE NANOCRYSTALS EXTRACTED FROM INDUSTRIAL HEMP AGRO-WASTE

2.1 Summary

Cellulose nanocrystals (CNCs) were produced directly from hemp agro-waste (HAW) using ammonium persulfate (APS) oxidation. Industrial hemp growth in the US has been accompanied with HAW production. While hemp has previously been shown as a source for CNCs, studies on CNCs from HAW (specifically hemp hurd) have not been reported on. Furthermore, studies on the mechanical characteristics of individual CNCs extracted using APS are lacking. Herein, the one-step oxidation treatment was followed by a purification step to remove impurities and hence to colloidally stabilize CNCs in aqueous suspensions, then analysis of the morphological and mechanical properties was performed. Purified and unpurified CNC samples were compared for potential differences in morphological and mechanical properties. Morphological analysis was performed using atomic force microscopy (AFM): purified CNCs had an average length of 183.1 ± 73.9 nm, unpurified CNCs had an average length of 202.0 ± 79.2, and both samples had an average diameter of 4 ± 2 nm. Mechanical analysis of individual CNCs using Force-Distance Spectroscopy (FDS) suggested both samples had little differences with average values of Young's modulus 2.19 ± 0.15 GPa, maximum loading force of 6.29± 0.09 nN, and adhesion energy of 1.57 ± 1.12e-16 J. No statistical differences between purified and unpurified CNCs were found in Young's modulus and maximum loading forces measurements, suggesting the impurities had minimum impact on mechanical strength. These results highlight the potential for mechanical assessment of individual CNCs extracted using APS from HAW via

FDS and the need for further exploration into the methodology of this type of mechanical analysis.

Key Words: Biowaste, Ammonium persulfate, Cellulose Nanocrystals, Atomic force microscope, Force/distance spectroscopy, Young's modulus of elasticity

2.2. Introduction

Cellulose is the most abundant and renewable organic material produced on the planet with current estimates of cellulose production at over 10 metric tons per year [1]. It is a semicrystalline material composed of crystalline and amorphous regions. Crystalline regions can be separated from each other by removing the amorphous regions, resulting in significantly small components known as CNCs which are considered as the building blocks of cellulose. CNCs are needle like in structure with diameters between 5-50 nm and lengths ranging anywhere from 100 to 500 nm [2] on average. CNCs have unique properties which make them valuable, including large aspect ratios, low density, water insolubility, desirable mechanical properties (large Young's modulus and tensile strength), biocompatibility, biodegradable, renewable, non-toxic, and have a highly modifiable surface [2–4]. CNCs natural occurrence in plant cell walls makes them a great source for sustainable and environmentally-friendly material [5]. Due to these unique properties, there are many applications for CNCs such as: antimicrobial/antiviral systems, tissue engineering, drug/gene delivery, modified drug release, biosensors, protein scaffold/biocatalyst, enzyme immobilization, water purification/waste-water treatment, supercapacitors, conductive films, sensors, energy storage, biodegradable plastics, food storage, and much more [6–8].

Wood is the primary source used for CNC production, however, CNCs have also been produced from cotton, alfalfa, tunicate, wheat straw, rice straw, sugarcane bagasse, algae, and more [9], making it a virtually inexhaustible resource. It has also been shown that CNCs can be extracted from hemp [10–13]. Recently, the '2018 US Farm Bill' has enabled the legal growth of hemp, a plant with some of the highest cellulose content (70-78%) next to cotton (65%) [14]. Hemp crop requires fewer fertilizers, herbicides, insecticides and water than cotton, increasing the number of states in the U.S. in which hemp can be grown. Furthermore, hemp provides higher

annual yields than cotton even with the requirement of little to no agrochemical input [15]. An increase in hemp production has recently occurred in the United States, resulting in both opportunities and challenges. One of these challenges is associated with agro-waste volume from hemp production. Biowaste production from industrial hemp growth highlights Hemp Agro-Waste (HAW) byproduct as a potentially underutilized source for large scale CNC synthesis.

Cellulose and CNCs can be extracted in various ways. Current methods for CNC synthesis include: subcritical water extraction [16], ball milling [17], high-intensity ultrasonication (Wang and Cheng 2009), acid hydrolysis, Ionic liquid [19], oxidation via TEMPO with homogenization [20], and oxidation using Ammonium persulfate [10]. The most common method for CNC extraction reported is acid hydrolysis, however, this method is not optimal. Acids create lots of hazardous waste, they are corrosive, and some biowastes require additional procedures prior to acid hydrolysis for CNC extraction. More environmentally friendly methods have been studied, such as subcritical water extraction and enzymatic extraction, but these methods require prior steps before they can be utilized effectively for the production of CNCs [16,21,22]. In 2011 the first article using APS oxidation was published, highlighting the use of a one-step method for CNC synthesis [10]. Since its original publication, the use of APS oxidation has increased in popularity [23–38] due to it being cheaper, more eco-friendly, having low toxicity, high solubility, no need for pretreatment, using a simple production process, and being less corrosive than other methods [37]. Upon heating APS, the peroxide bond is cleaved resulting in two SO_4^- radical ions; simultaneously hydrogen peroxide (H_2O_2) is formed. Together these compounds oxidized CH_2OH located at the C6 position, removing the amorphous regions of cellulose [23] and releasing the crystalline regions of cellulose. This one-step method not only requires fewer chemicals and

the byproducts from the reaction process can be recovered allowing for responsible waste management. APS produces two main by-products, sulfate ions (H_2SO_4) and ammonium sulfate (AS). With the NH_4OH to neutralize the reaction and then precipitation with $EtOH$ allows for recover of AS [23]. Being able to recover waste products reduces hazardous waste and introduces the potential for large scale production via chemical synthesis, making it a more environmentally friendly procedure that can support the extraction of CNCs from biowaste.

Applications of CNCs require a knowledge of the source material and its impact on these nanoparticles. CNC properties can vary depending on what they were extracted from [39,40] and the method in which they were extracted [41]. These manifest in the form of different sizes, potential differences in the surface chemistry, and changes in mechanical properties. While size and morphology of CNCs have been studied thoroughly from various sources using different synthesis methods, mechanical properties are an area that could use further research. Methods for mechanical property evaluation of nano particles and nano fibers currently include: Raman Spectroscopy [42], X-Ray Diffraction [43], Inelastic X-Ray Scattering (IXS) [44], AFM – Scanning Electron Microscopy (AFM-SEM) [45], AFM – 3 point bending (AFM-3PB) [46–48], AFM – nano indentation (AFM-NI) [49], AFM-FDS (Wagner, Raman, and Moon 2010). While there are other methods for determining the characteristics of nanoparticles, AFM has shown to be a powerful tool for use in the micro and nanoscale world. AFMs can easily assess size, morphology, and mechanical characteristics with great accuracy, making it a more suitable candidate for evaluating the characteristics of individual CNCs. Of the methods used by AFMs for measuring mechanical characteristics, AFM-3PB has been one of the more recognized. However, methods for creating grooves to suspend the nanoparticles across is required. Current manufacturing methods are hard-pressed to make grooves smaller than 227 nm across [46–48], therefore, using

AFM-FDS is a more feasible option to readily test mechanical properties of CNCs smaller than 300 nm in length (Wagner, Raman, and Moon 2010). To date there have been no articles published on the mechanical properties of CNCs extracted from hemp. Furthermore, there have been no publications on the mechanical properties of CNCs extracted using the one-step APS oxidation method.

The work reported hereby successfully demonstrates the extraction of CNCs from HAW, specifically hemp hurd, using a one-step APS method. The results of this study show that HAW is a potentially viable option for large scale CNC synthesis. In conjunction with the ability to recover waste byproduct materials, discussed in previous literature [23], using a post processing method, this study further suggests the potential of decreasing the ecological impact of industrial hemp growth/waste in America by using it as a source of CNC synthesis. This study also highlights the mechanical properties of CNCs derived from HAW found using AFM-FDS for suspended CNCs as well as CNCs lying flat on a surface. Specifically, AFM-FDS was used to evaluate Young's modulus, adhesion energy, and maximum load. Limitations of the AFM-FDS method are summarized and the results point to the usefulness of more thorough testing for validation of this mechanical testing method on CNCs.

2.3. Materials and Experiments

2.3.1 Materials

Raw Hemp (*Cannabis Sativa* L.) hurds, collected from HAW after fiber removal via retting and mechanical separation, were donated by a local hemp farm (Fort Collins, CO). The as received hemp hurds were processed using a mechanical blender (Cincred MC-BL618) into fine powder. Ammonium Persulfate (≥98%, Aldrich) was purchased from Sigma Aldrich and Sodium

Hydroxide (99.4%, Fisher) purchased from Fisher Scientific. All chemicals used were of reagent grade and used without further purification.

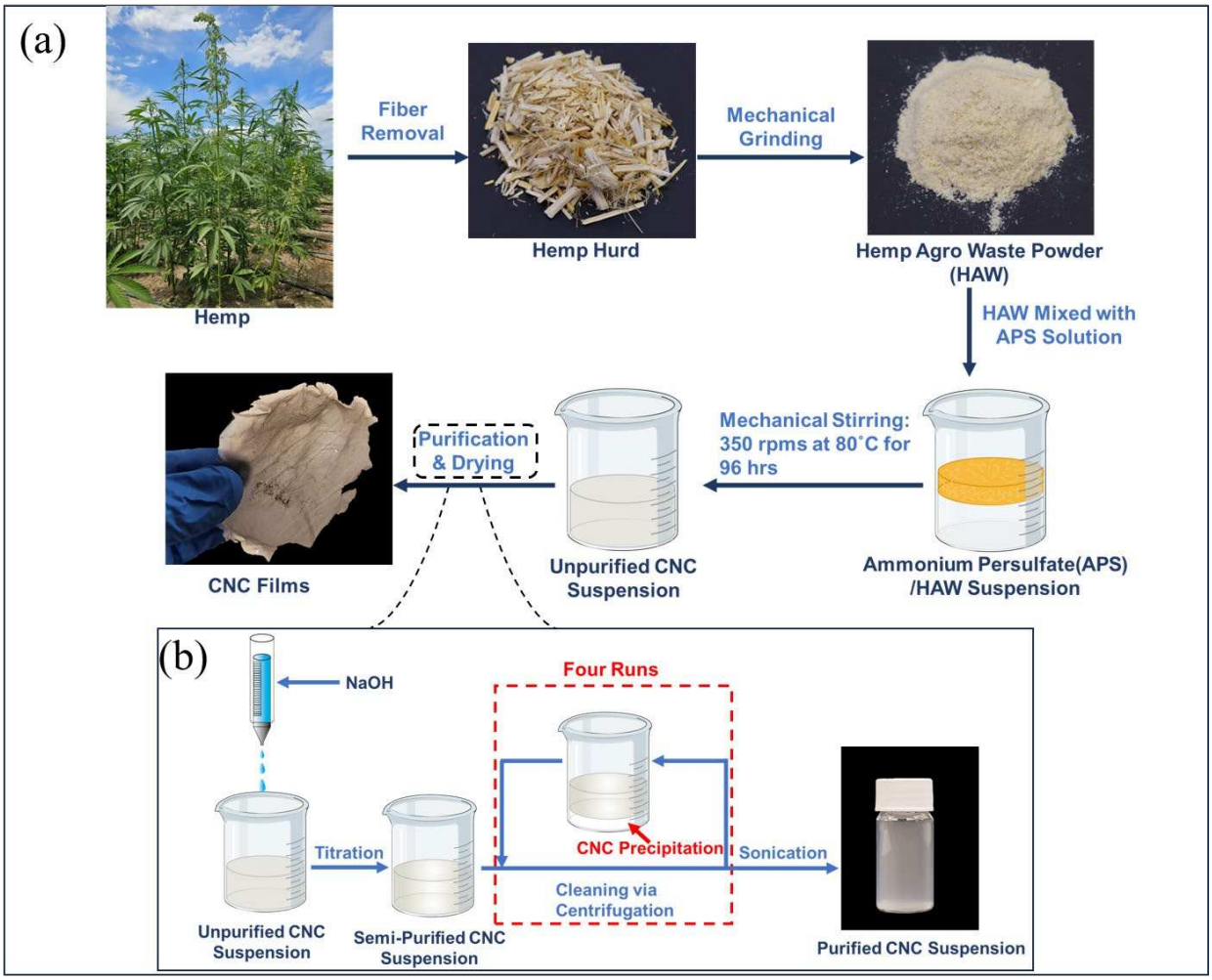

Figure 2.1: Synthesis of cellulose nanocrystals from hemp agro-waste: (a) Major synthesis steps and (b) Purification process.

2.3.2 Synthesis of CNC Nanoparticles

APS treatment was a method previously reported by Leung et. al [2011]. Hemp hurd was used as the starting material and ground down to make a fine HAW powder. 2 grams of raw HAW powder was added to 100 mL of 46% w/v (2 M) APS solution. The mixture was heated to 80 ˚C and mechanically stirred continually at 350 rpm for 96 hours. The suspension was collected using a centrifuge at 6000 rpm for 15 minutes. Supernatant was decanted, distilled

H_2O was then added to CNC tube and resuspended using vortex machine till thoroughly mixed, and then centrifuged for 15 minutes. Wash cycles were performed 4 times or until pH 4 was reached resulting in an unpurified CNC (UP-CNC) product (Fig. 1a).

The purification process began by collecting UP-CNCs and resuspending them in distilled water. CNC/water suspension was brought to pH 7 using 1M NaOH added drop wise and was closely monitored using an electronic pH meter (OAKTON pH700). Suspension was put through a second round of wash/centrifuge cycles. Collected CNCs were resuspended in distilled H_2O by ultra-sonication (Fisher Scientific FB-505) in an ice-bath using a 1/8" probe (Fisher Scientific FB4418) at 30% of max amplitude (500 Watts at 6 kHz) for 15 minutes (Fig. 1b). Final product was poured onto hydrophobic surface and placed in desiccator until completely dried. Three different samples were prepared for further analysis: (i) HAW in powdered form, (ii) UP-CNC, and (iii) purified APS treated CNC (P-CNC).

Percent yield was determined by using the final dried weight of the collected CNCs and dividing it by the percent content of cellulose in the HAW powder. The calculation was performed using equation 1:

$$\%yield = \frac{dry\ CNC\ weight\ (g)}{HAW\ powder \times \%cellulose\ content\ (g)} \times 100 \quad (1)$$

2.3.3 Chemical Analysis

CNC chemical structure was evaluated using attenuated total reflectance-Fourier transform infrared spectroscopy (FTIR, Agilent Cary 630). FTIR spectra were recorded in 4000-650 cm^{-1} range with resolution of 2 cm^{-1} and an accumulation of 32 scans. In addition, element analysis of samples was performed using a Scanning Electron Microscopy and Energy Dispersive X-ray Spectroscopy (SEM-EDS, JEOL JSM-6500 Field Emission Scanning Electron

Microscope). A UP-CNC thin film sample was placed on carbon tape, due to the sample having been pre-dried before analysis, and a P-CNC sample was measured on a silicon wafer substrate, due to the sample being in solution prior to analysis. P-CNC, with a concentration of 2% w/v, was dried onto silicon wafers using a drop-casting method. UP-CNC thin film was directly placed on carbon tape. Gold sputter-coating was performed for 15 seconds to deposit a 10 nm thin film on samples prior to analysis (Denton Vacuum Desk II). SEM-EDS was then used to determine the specific makeup of UP-CNC and P-CNC samples to check for major differences in element composition.

2.3.4 Crystallinity Measurement

X-ray Diffraction (XRD) measurements were obtained on a Bruker D-8 Discover DaVinci X-ray diffractometer. HAW, P-CNC and UP-CNC samples were scanned with (Cu-Kα X-ray source, line focus) radiation in the 2θ range of 5-80˚. The crystallinity index (CrI) was calculated according to Segal's Equation:

$$CrI = \frac{(I_{200} - I_{am})}{I_{200}} * 100 \qquad (2)$$

I_{200} is the peak intensity at 200 and I_{am} is minimum point between the 110 and 200 peaks. All samples were further analyzed using DIFFRAC.EVA v.6.0 software in conjunction with globally recognized databases accessed by the software to asses all peaks from samples for all possible crystal structures.

2.3.5 Size and Morphological Characterization

The particle size and zeta potential of CNCs were analyzed (Malvern Instruments Zetasizer Nano ZS). Dynamic light scattering (DLS) using a DTS0012 disposable cuvette was performed to assess the hydrodynamic radius of CNCs. Two samples were prepared before

measurements: (i) UP-CNC and (ii) P-CNC, by suspending CNCs in distilled water at room temperature at pH 7. Suspensions were diluted to concentrations of 0.0002% w/v. Tests on samples were run in triplicates and the means were averaged together. Mix-mode measurement phase analysis light scattering (M3-PALS) was performed using a DTS1070 disposable capillary cuvette for zeta potential measurements. An aqueous suspension of P-CNC in distilled water at a concentration of 0.0002% w/v, pH 7, and at room temperature was prepared. Measurements were performed in triplicate and the means were averaged.

In addition, AFM (Park Systems XE-70) was performed for dimension analysis. Two CNC aqueous dispersions were used for this study: (i) UP-CNC suspension and (ii) P-CNC suspension. UP-CNC and P-CNC samples were diluted to concentration of 0.002% w/v. The diluted samples were then dropped onto separate optical glass slide covers and dried in the air. The dry samples were scanned at room temperature using both contact and non-contact modes. Non-contact cantilever (Park Systems OMCL-AC160TS) and contact cantilever (Park Systems CONTSCR) were used for imaging. Before evaluation of CNC morphology, XEI-70 was calibrated for accuracy. Proprietary XEI software (Park Systems) was used to measure the height of CNC particles. Images collected were then used to analyze the length and width of P-CNC and UP-CNC using ImageJ for further dimensional analysis of CNCs.

2.3.6 Mechanical Analysis

Mechanical characteristics for agglomerated and single CNCs were tested on the AFM using FDS (Park Systems XE-70). Four different Samples were prepared for FDS analysis: (i) unpurified Agglomerated CNCs, (ii) purified agglomerated CNCs, (iii) unpurified single CNCs, and (iv) purified single CNCs. Each sample underwent mechanical testing using a contact cantilever (Park Systems CONTSCR). All CONTSCR cantilevers used had a tip radius of

curvature <10 nm and a spring force constant possessing nominal values of 0.2 N/m. Before FDS measurements were taken of the CNC samples, the glass substrate was tested to identify the mechanical forces of the substrate itself. This step was done to verify that FDS measurements were taken of CNC particles only. Measurements of CNCs in agglomerated samples were taken at varying locations along their axis, avoiding locations of direct overlap, for at least 50 random CNC particles. Measurements of single CNCs were taken by locating particles that had no overlap with another particle and were flat on the glass substrate. At least 50 measurements were taken of single CNCs to ensure reasonable distributions. A new contact cantilever was used for each sample to ensure that measurements of each sample was not skewed due to tip deformation from previous samples. During FDS the XEI software measured Young's modulus (E), maximum force (N), and adhesion energy (J), and the average and standard deviation were calculated from these results. P-CNCs and UP-CNCs were tested using two distinct groups: agglomerated particles and single particles.

Statistical analysis was conducted for the mechanical properties: Young's modulus (E), maximum force (N), and adhesion energy (J). Two-way ANOVA and Tukey multiple range tests were performed using Rstudio statistical software. Analysis and comparisons of purified vs unpurified samples for Agglomerated and Single CNC particles were made. Results for Young's modulus (E), adhesion energy (J), and maximum load (N) all underwent statistical analysis.

2.4 Results and Discussion

This study assesses the impact remaining residues from the extraction process have on CNCs. For many applications, especially in the medical field, CNCs may be introduced to various media prior to application. This brought up the question, does the presence of other substances around CNCs alter their mechanical properties? CNCs were extracted from HAW

using the modified APS method shown in Fig. 1. Hemp hurd has a cellulose content of 40–48% [51]. Using this range the CNC yield was calculated to be between 3.06-3.68%, which was done using equation 1 located in the materials and methods section. Hemp fibers used for extracting CNCs via APS treatment reported a percent yield between 26-36% [10]. Percent yield found by the extraction of CNCs from Jute fiber using APS were found to be 64%, 61%, 57%, and 54% for rection times of 6 hours, 8 hours, 12 hours, 16 hours, and 24 hours, respectively [29]. This highlights the role extraction time plays in CNC yield and could potentially elucidate the cause of such a low yield for our experiment.

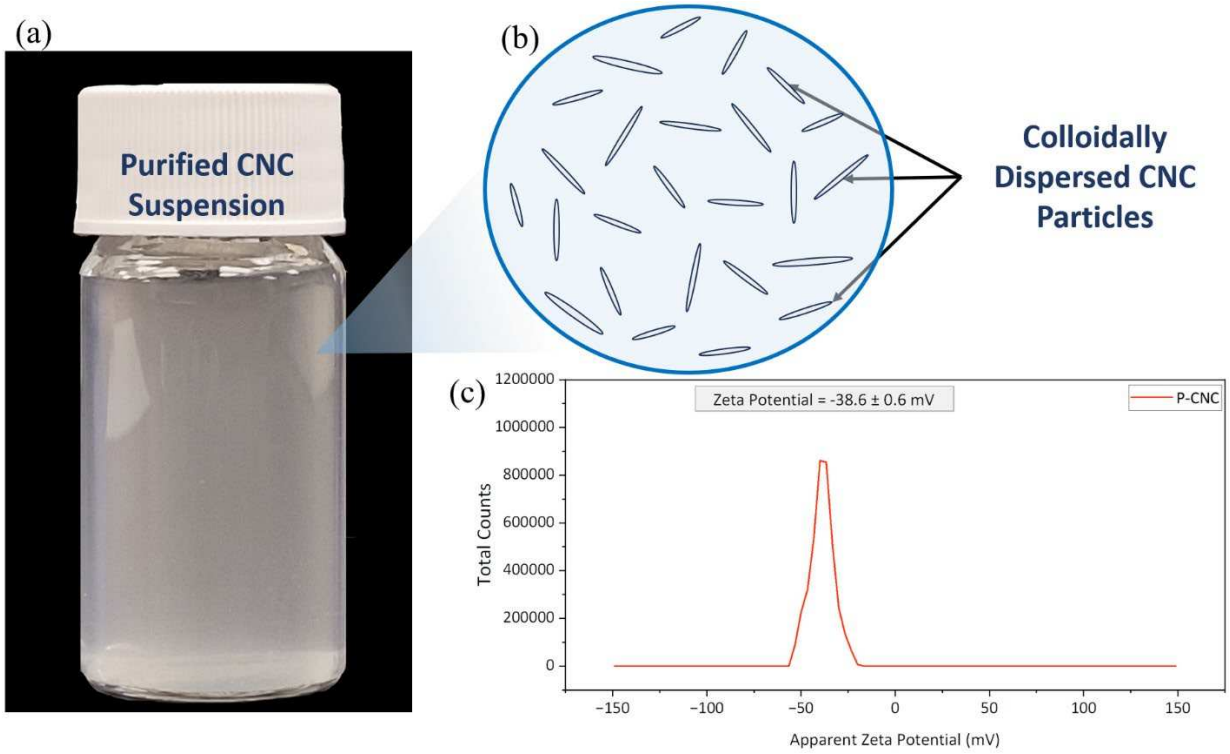

Figure 2.2: Zeta potential for colloidally stable CNC particles in water; (a) Purified CNC suspension, (b) Graphic of purified CNCs in water, and (c) Distribution of zeta potential for CNC.

Zeta potential measured using M3-PALS was used to determine the stability of our particles. It has been reported that nanoparticles with a Zeta Potential lower than -25 mV are colloidally stable in a suspension [35]. CNCs extracted from various sources have been reported to

be colloidally stable [10,13,25,40,41,52–55]. Fig. 2 illustrates the uniform dispersion of CNCs throughout the purified CNC suspension after three days. Evaluation of long-term colloidal stability in suspension will be further investigated in future work. It can be seen in the image that the CNC aqueous suspension is homogeneous and absent of any visible aggregates, suggesting colloidal stability. Analysis of zeta potential measurements by M3-PALS gave a value of -38.6±0.6 mV for P-CNC. Other research groups that have used APS oxidation report zeta potentials between -30 mV and -40 mV [29,30] which are in agreement with the zeta potential in this study. Note, analysis of UP-CNC zeta potential was not performed. Due to M3-PALS sensitivity to parameters such as pH, the medium in which the particles are suspended, ionic strength, and concentration of the suspension [56], contamination of UP-CNC may prevent accurate measurement of the CNC surface charge. Detailed analysis into the contaminants of the UP-CNC samples is required to take into account how CNC surface potential is impacted and determine with relative accuracy the actually surface charge, which was outside of the scope of this work.

2.4.1 Chemical and Elemental Composition

Cellulose chain molecules are compose of many glucose residues linked by β-1,4-glycosidic bonds creating a linear homopolymer [40] which can be categorized into one of four major polymorphic forms: I (containing sub-allomorphs Iα and Iβ), II, III (containing sub-allomorphs III_I and III_{II}), and IV (containing sub-allomorphs IV_I and IV_{II})[40]. Higher order plants have cell walls that are rich in Iβ but also contain small amounts of Iα [3]. HAW, UP-CNC, and P-CNC samples were characterized via their chemical composition and surface functionality using FTIR spectra shown in Fig. 3a. All three samples showed characteristic cellulose peaks at 3312 cm^{-1} and 2881 cm^{-1} which represent the stretching vibration of -OH groups and CH- groups [13,29,31,33,35] respectively. HAW sample has noticeable peaks at 1729 cm^{-1} and 1234 cm^{-1} (Fig.

3a) that are typically associated lignin [33] and hemicellulose [57,58], respectively, but are not present on P-CNC sample. Interestingly, a peak at 1729 cm^{-1} can be seen in the UP-CNC sample, this could imply that a trace of lignin was still present in the sample before NaOH treatment was applied for thorough cleaning. The intense peak at 1604 cm^{-1} is indicative of the presence of $-COONa$ [13] that occurred during NaOH treatment [23] of the UP-CNC during the final CNC purification process. Presence of peaks at 1420 cm^{-1}, 1160 cm^{-1}, 1102 cm^{-1}, 1022 cm^{-1}, and 891 cm^{-1} are in line with previous studies suggesting those representative of cellulose [13] and to be more specific, cellulose Iβ [23].

The FTIR results show that P-CNC has more intense and well-defined peaks than the other samples, which could be indicative of the potential purity of cellulose within the sample. The findings shown are in line with literature, confirming the successful synthesis of CNC from HAW. To verify the results found in FTIR analysis concerning the peak at 1604 cm^{-1}, samples were analyzed using SEM-EDS. Fig. 3b and 3c show an element map spectrum for UP-CNC (Fig. 3b) and P-CNC (Fig. 3c), respectively. There is a large spike of Na on the P-CNC graph, suggesting the formation of $-COONa$ on the CNC surface during NaOH treatment, which has been previously reported [23]. It is interesting to note the presence of chlorine in the P-CNC sample. UP-CNC has a higher carbon concentration than P-CNC. This higher amount of carbon to oxygen ratio could potentially be related to the carbon tape that the sample was placed on, depending on the depth of penetration during sample measurement and the thickness of the UP-CNC film. It should be noted that there is a small peak of silicon on the P-CNC, which is likely from the silicon wafer substrate used to prepare the P-CNC sample for SEM-EDS measurements. However, the UP-CNC also had a large peak representative of silicon. Because the UP-CNC was deposited on a caron tape, not a silicon wafer, there might have been some contamination during

CNC extraction prior to purification. Both samples show significant peaks from gold due to the samples undergoing gold plating before SEM analysis.

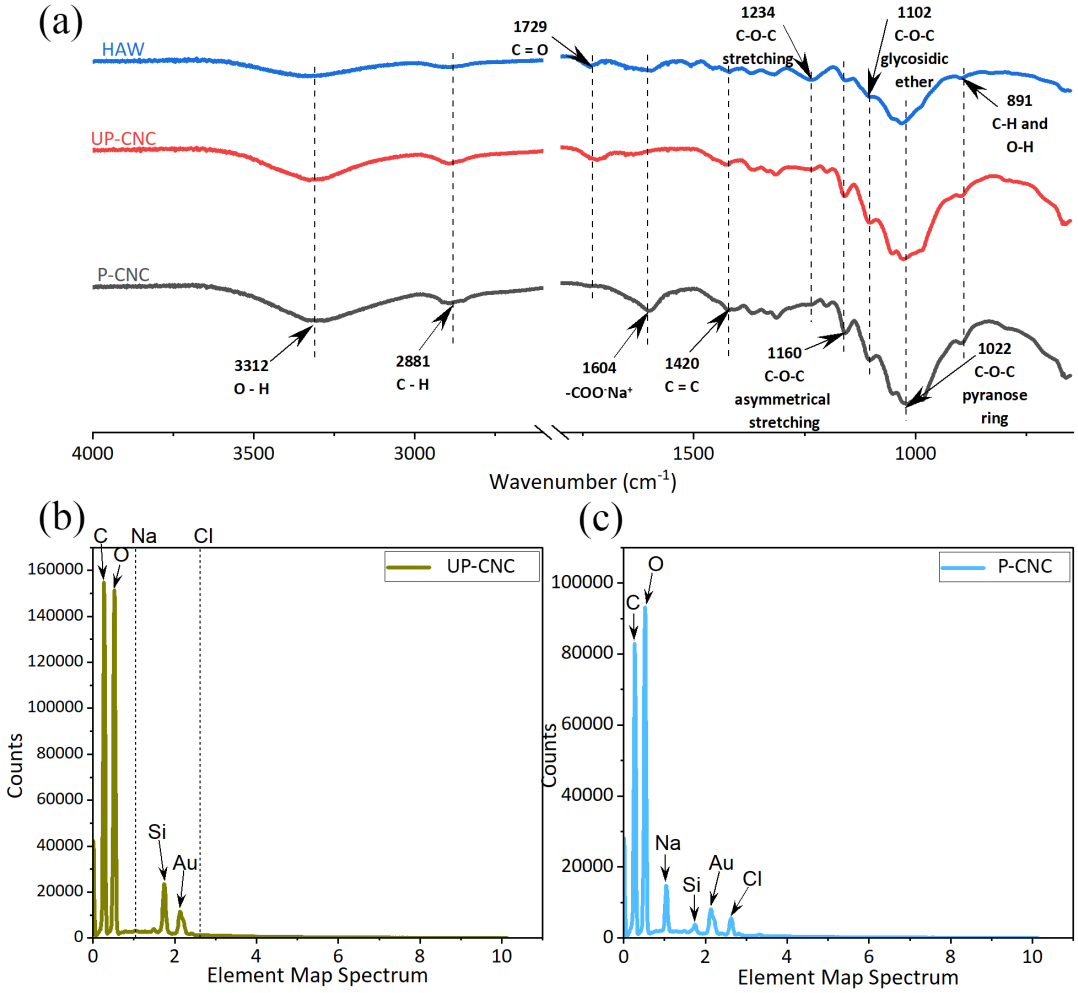

Figure 2.3: Chemical and Elemental analysis of CNCs: (a) FTIR spectra, (b) SEM-EDS of UP-CNC, and (c) SEM-EDS of P-CNC.

Crystalline structure and crystallinity were analyzed using XRD and the results are shown in Fig. 4. The spectra for HAW, UP-CNC, and P-CNC were recorded and the CI was determined. There are six types of allomorphs of cellulose [40]. Native cellulose found in most plants is comprised of cellulose I and is found as a combination of suballomorphs Iα and Iβ [2]. HAW is primarily composed of cellulose Iβ, which is confirmed by the primary peak at 22.7° , 16.5°, and 15.1° [23].

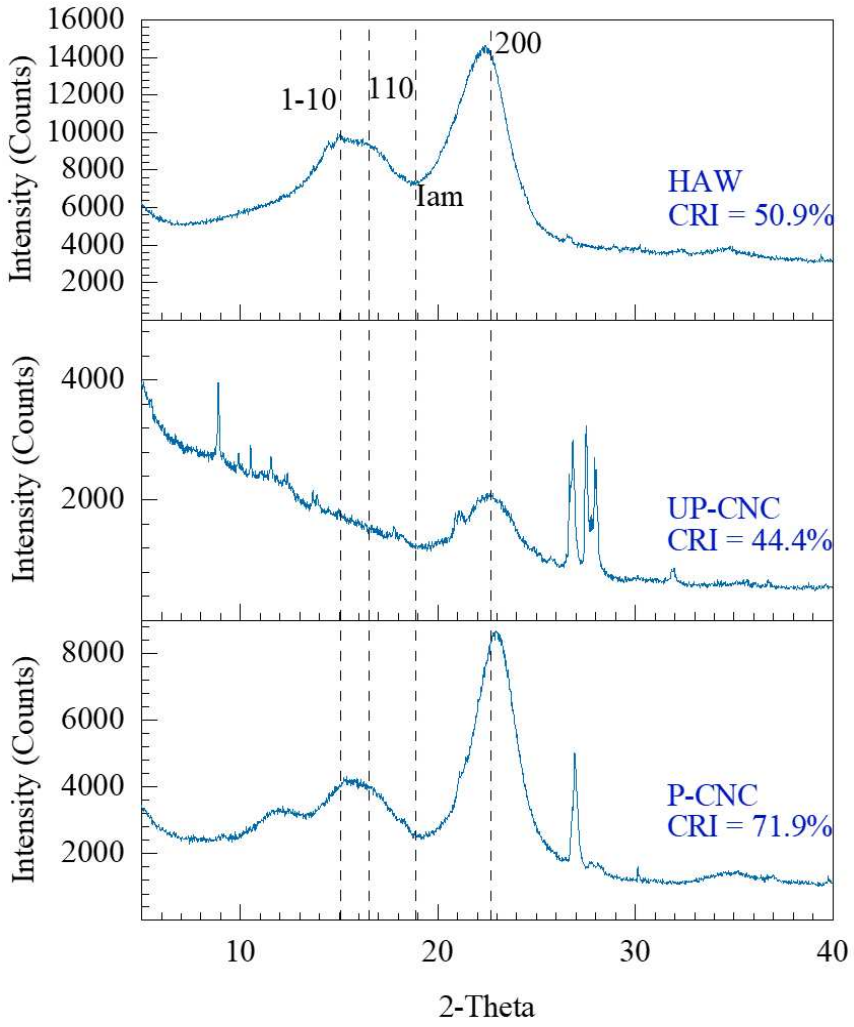

Figure 2.4: XRD graphs for HAW, UP-CNC, and P-CNC samples.

In addition, the ratio of Iα and Iβ is dependent on the source plant. Further analysis of P-CNC suggested that cellulose Iβ was the primary cellulose suballomorph composing P-CNC, which is in line with previous reports on higher plant cellulose composition [40]. The crystallinity Index (CrI) for HAW, UP-CNC, and P-CNC samples were found to be 50.9 %, 44.4 %, and 71.9 %, respectively. The purification improved the CI of CNCs by 27.5 %, suggesting the importance of purification in the CNC extraction. Of note there is a sharp peak at 2θ = 26.9˚ that upon investigation pointed to the possible presence of two potential candidates: sulfur oxide amide ($S(NH_2)_2O_2$) and hydrogen ammonium sulfate sulfamate ($H(NH_4)_2(SO_4)(SO_3NH_2)$). Furthermore, P-CNC has a peak at 12˚ and a visible "shoulder" at approximately 21˚ which

correspond to 1-10 and 110, respectively, suggesting the potential presence of cellulose II in this sample as well. The UP-CNC sample had a primary peak at 22.7˚ that was significantly lower than the other two samples and was missing a distinct peak at 15.1˚. Also, of note for the UP-CNC sample is the presence of sharp peaks at 26.9˚, 27.5˚, and 27.9˚ that are not in line with HAW and P-CNC, which was likely due to the lack of thorough cleaning of the UP-CNC sample. Investigation into these impurities illuded to the possible existence of Sulfur Oxide Amide ($S(NH_2)_2O_2$) and cellulose II in the sample. The potential presence of cellulose II in the UP-CNC sample could be due to a chemically induced gradual change of the crystal lattice from cellulose I to cellulose II [2]. However, it is important to note the lack of sulfur molecules in the EDS analysis. Due to limitations using XRD and FTIR, resulting in poor characterization of UP-CNC, more research would be required to determine the potential presence of sulfur containing compounds and cellulose II in future work.

2.4.2 Size and Morphology Analysis

Fig. 5 includes size distributions of the hydrodynamic radius of CNC particles for P-CNC (Fig. 5a) and UP-CNC (Fig. 5b) samples, as well as depictions representing these suspensions (Fig. 5c and Fig. 5d). DLS measurements found the hydrodynamic radius of CNC particles for the P-CNC and UP-CNC samples were 151.6 nm and 173.2 nm respectively, shown by Fig. 5a and Fig. 5b respectively. The size distributions were found using particle intensity and displayed in Fig. 5 showing that the P-CNC samples (Fig. 5a) had more consistent measurement overlap than the UP-CNC samples (Fig. 5b). Consistent overlap of the P-CNCs confirms that the purification process is valuable in the removal of unwanted materials other than cellulose. However, Fig. 5a shows that there were larger particles (900 – 2000 nm) present in the P-CNC solution. This is most likely from agglomeration of CNC particles due to difficulties surrounding

redispersion in water after they have been dried at the end of the APS method [53]. On the other hand, the UP-CNCs were easier to redisperse after drying, potentially preventing large agglomerations of CNCs (Fig. 5b). Redispersion of UP-CNCs may be due to residues present reducing adhesion between CNC particles.

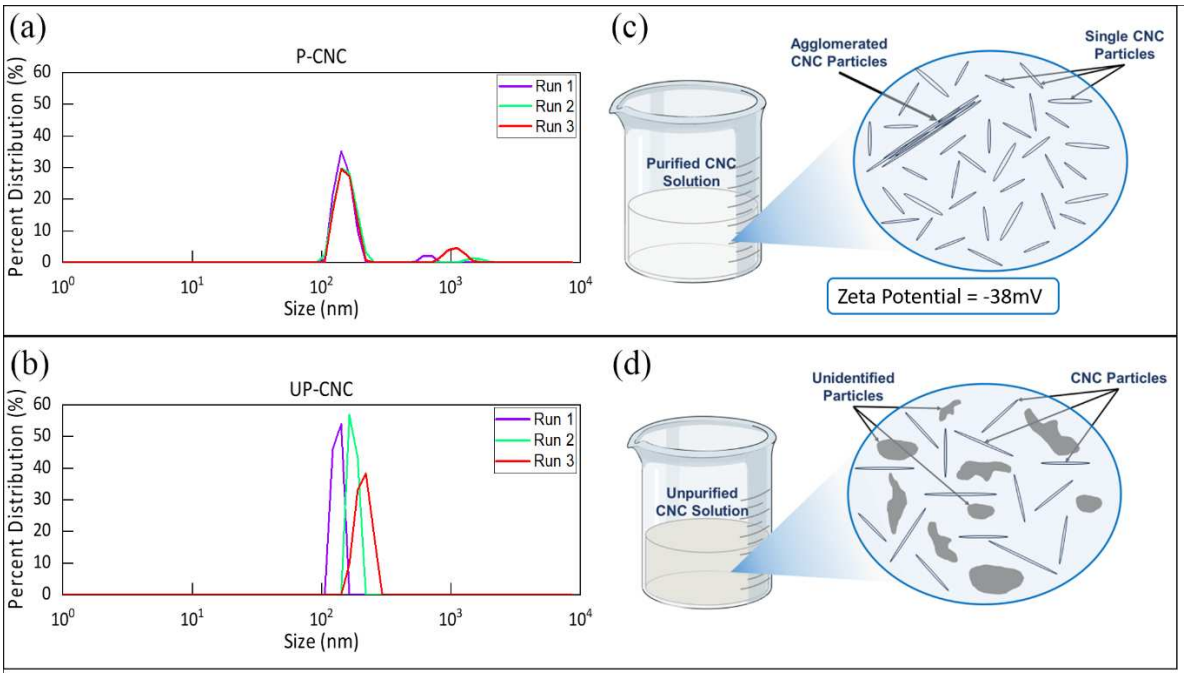

Figure 2.5: DLS size distribution of CNC were analyzed using multiple runs on each sample. Measurements were performed on two samples and the size distributions are shown: (a) P-CNC size distribution and (b) UP-CNC size distribution. Visual representations of the individual solutions shown: (c) P-CNC graphic including CNC Zeta Potential and (d) UP-CNC graphic.

AFM Images of both P-CNC and UP-CNCs shown in Fig. 6 suggested that the CNCs derived from hemp are needle-like in shape, which is in a good agreement with previous reports [13,59]. Fig. 6a and 6b are good representations of the average CNCs found using topographical and force imaging techniques, respectively, on the AFM. The length and width of P-CNC and UP-CNC size distributions are shown in Fig. 6d. However, convolution of the tip shape in conjunction with the sharp edges of the nanocrystals can make the width of CNCs appear to be

much larger than what they truly are [59], therefore it is best to estimate width using the AFM height [25].

Fig. 6c shows multiple graphs, measured with the line function via the XEI software, depicting the height profiles (actual widths) of CNCs. Lines (i, ii, and iii in Fig. 6c) were drawn over areas with as little overlap as possible to accurately show the heights of individual CNCs. This was done with multiple images (not shown in this text) to ensure consistency and accuracy of measurements. The measured height of individual P-CNCs and UP-CNCs range between 2 to 6 nm. Both UP-CNCs and P-CNCs had an average height of $4 \pm 2\ nm$. Length and width of CNCs were separated into their respective groups, P-CNC and UP-CNC and the mean was determined by averaging over 200 CNCs for each group using ImageJ. The average length was $183 \pm 74\ nm$ and $202 \pm 79\ nm$ for P-CNC and UP-CNC, respectively. The average width was $29 \pm 10\ nm$ and $27 \pm 9\ nm$ for P-CNC and UP-CNC, respectively. As previously stated, due to tip convolution it is hard to known the true width of the CNCs. Therefor we used the average height instead of width and the average length for each sample to calculating the aspect ratio. The average aspect ratios were calculated to be 30 for P-CNC and 33 for UP-CNC. These results are similar to other reported aspect ratios for hemp extracted using APS oxidation [13], cotton extracted using acid hydrolysis, and tunicate extracted using acid hydrolysis [40]. It was reported by Leung et al. that hemp-derived CNCs measured using AFM have an average length of 148 nm and average diameter of 5.8 nm. Vanderfleet and Cranston (2020) also reported lengths between

100 nm - 200 nm for CNCs using sulfuric acid hydrolysis. Morphological results found in this study are on par with those previously reported [13,23,40,60].

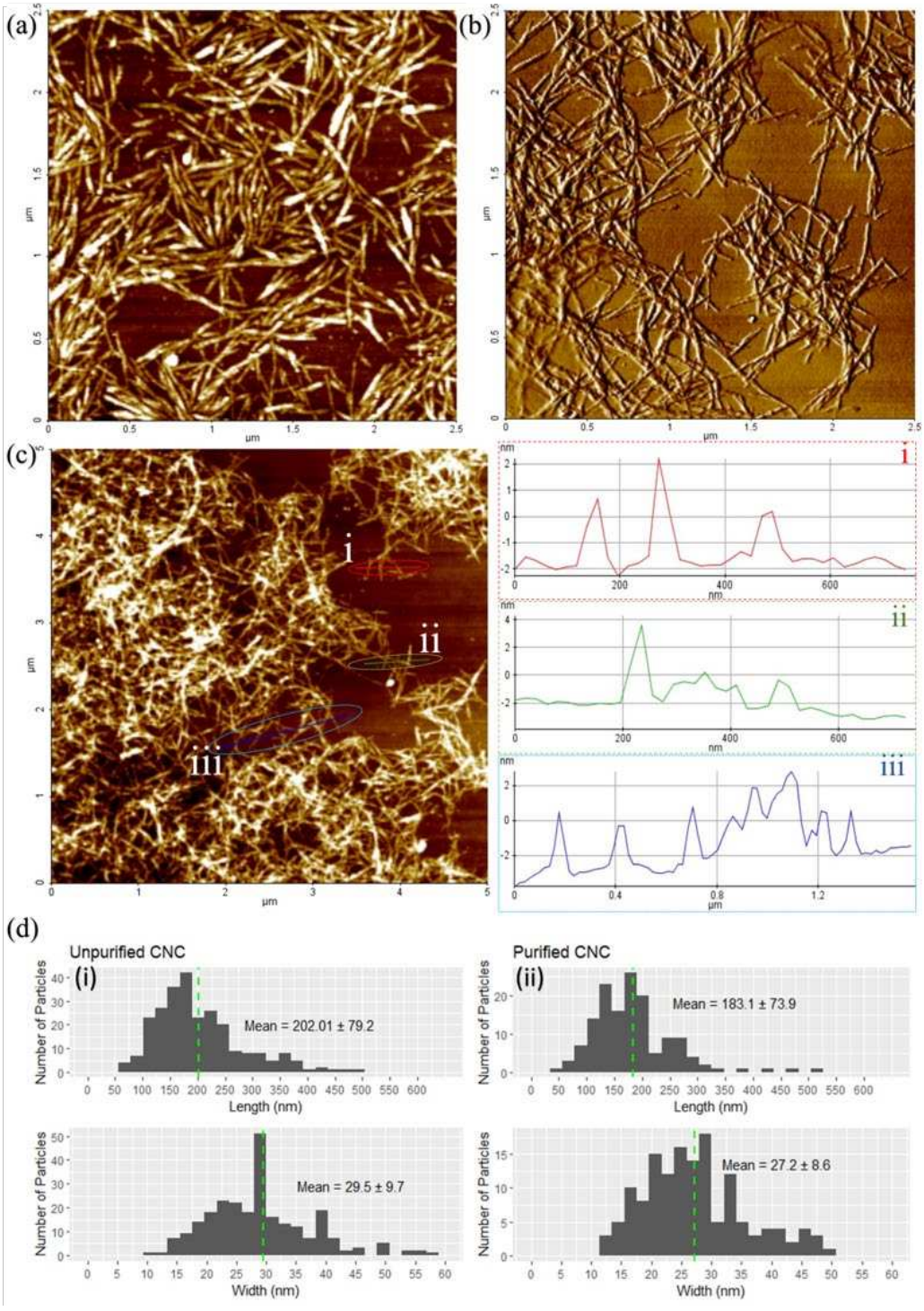

Figure 2.6: AFM images with size distributions of CNCs derived from hemp waste. (a) Topology image taken from UP-CNC sample, (b) Force image taken from P-CNC sample, (c) Topology for

field of CNCs with height profile graphs (i, ii, and iii), and (d) Length and width size profile histograms of UP-CNC samples (i) and P-CNC samples (ii).

2.4.3 Mechanical property analysis

FDS using an AFM (Fig. 7) was employed to study mechanical properties of the hemp-derived CNCs. This method can be split into 3 parts: (i) the approach of the needle to the surface of the particle shown in Fig. 7a, (ii) the downward depression of the needle onto the particle shown in Fig. 7b, and (iii) the upward retraction from the particle depicted in Fig. 7c. The overall process generates a force/distance curve that can be used to measure the Young's modulus (Pa), adhesions energy (J), and maximum applied load (N) of the particle. Maximum force refers to the force that was applied by the cantilever during indentation, and this value is dependent on the stiffness of the cantilever [48]. Adhesion energy is the energy required for the tip of the cantilever to detach from the sample surface upon retraction. The results from our mechanical analysis are shown in Fig. 7 (f), (g), and (h), respectively. Large error bars found in most of the FDS measurements are likely due to locations of sampling taken along a 'suspended' CNC in large agglomerations.

First, the maximum load (~6.3 nN) applied to the four samples, shown in Fig. 7e, were statistically similar. However, the unpurified-agglomerated (UP-CNC-A) sample was noticeably lower than the other samples. This lower value (~6.15 nN) of the UP-CNC-A sample is most likely due to the presence of impurities within the sample, allowing more compression to occur at a lower load. Second, the adhesion energy (Fig. 7f) has statistically significant differences among all four samples with the purified-agglomerated (P-CNC-A) sample having the largest average value of 2.83E-16 J and the UP-CNC-A sample having the lowest average value of 3.40E-17 J. This attractive force is most likely the cause of larger reported adhesion energy. However, the lowest adhesion energy measured was that of the UP-CNC-A sample. Such drastic

differences between samples containing agglomerated CNCs may be due to the impurities within the unpurified sample obstructing the attractive forces between the CNCs and ultimately reducing the overall adhesion energy.

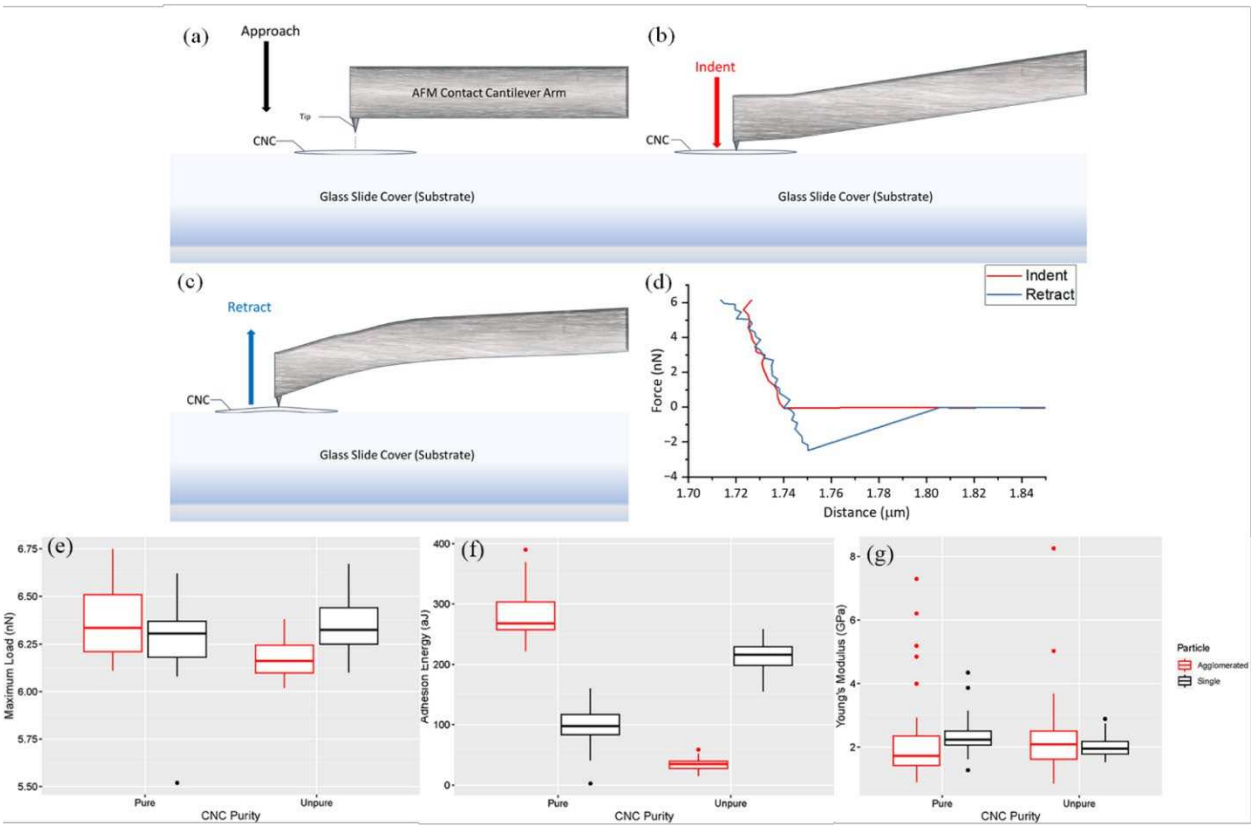

Figure 2.7**:** Force/distance mechanical measurement and measured mechanical characteristics of CNC: (a) AFM cantilever approaching CNC, (b) AFM cantilever upward deflection during indentation, (c) AFM Cantilever downward deflection during retraction, (d) Force/distance spectroscopy curve measurement, (e) Maximum applied load (nN) of cantilever applied to CNC, (f) Adhesion energy (aJ) between CNC and cantilever, and (g) Young's modulus (GPa) of CNC. CNCs are known to agglomerate when they dry due to attractive forces between the particles [3,53].

It is important to note that the second lowest adhesion energy of 9.71E-17 J was that of the purified-single CNC (P-CNC-S) sample. This low adhesion energy is most likely due to the lack of attractive forces between the glass substrate and the CNCs with minimum impurities. Lack of

attractive forces between the substrate surface and CNC surface would impact the reported adhesion energy by noticeably decreasing it.

Lastly, Young's modulus was of most interest (Fig. 7g). Young's modulus for CNCs is separated into two distinct directions: (i) Transverse elastic moduli (E_T) which is measured perpendicular to the chain axis (along the cross-section of the CNC) and (ii) Axial elastic moduli (E_A) which is measured parallel to the chain axis (Lahiji et al. 2010) (along the length of the CNC). E_A for CNCs has been reported by multiple sources to be between 110 – 200 GPa both theoretically and experimentally [61], however, it should be noted that there were no current sources that include reports for either E_T or E_A of hemp sourced CNCs. Methods for experimentally measuring E_A include: Raman spectroscopy, combining AFM and SEM, FDS with AFM, w/H bonding, wave propagation, and X-ray diffraction [47,48,61,62]. AFMs are primarily used to find E_T one of two ways: (i) using FDS (Abbasi Moud 2022; Lahiji et al. 2010; Iwamoto et al. 2009; Wagner, Raman, and Moon 2010) or (ii) Nano-Indentation [63]. Nano-indentation can be used for determining elastic-plastic behavior of nanorods, nanowires, and nanofibers, but due to difficulties with probing curved surfaces, it is not widely used or studied [63]. Therefore, the Young's moduli shown in Fig. 7g are the E_T of the hemp-derived CNCs. The average recorded value of E_T for all four samples is between 2 and 2.3 GPa. Values around 2 GPa are in line with reported theoretical estimates of E_T between 2 and 37 GPa, reported for CNCs derived from tunicates (Wagner, Raman, and Moon 2010). It is known that CNC mechanical properties can vary depending on the source or the method of synthesis [4,39,41]. Differences are found not only in the morphology of the particles but also in other characteristics such as thermal stability [64], chemical properties [64], and mechanical properties [59]. For example, a method similar to the one used in this study was performed on a single tunicate CNC on a mica substrate using FDS and

reported an E_T of 9 GPa with a standard deviation of 2 GPa (Wagner, Raman, and Moon 2010). Fig. 7g shows large deviations for both agglomerated samples with values as high as 8 GPa, which is within the range of tunicate CNC reported previously (Wagner, Raman, and Moon 2010). Of note, these large deviations in measured E_T may have to do with the location along the length of suspended CNCs that measurements were taken [48]. Interestingly, there were no statistically significant differences found among all four samples (agglomerated and single particles), which is in good agreement with previous reports using cantilevers that had maximum load below 10 nN [48]. Therefore, the current measurements of E_T were within an acceptable theoretical range. In comparison with the current measurement on E_T using FDS on an AFM, a 3-point-bending method has been previously reported to have rod-like nanoparticles such as CNCs' mechanical analysis which requires the particles to be placed over gaps on the substrate surface [47]. However, it has been reported that E_T can still be measured for particles without undergoing 3-point-bending tests (Wagner, Raman, and Moon 2010), graphical depiction of this model shown in Fig. 7(a-c). Another study was performed on the properties of the cantilevers used for FDS and their impact for experiments on nanofibers [48], suggesting that the cantilevers with lower stiffnesses that are unable to accommodate maximum load forces greater than 10 nN do not show significant differences between particles on the substrate versus those above a groove [48]. Fig. 7d shows a typical force/distance profile of the CNC measured using a contact cantilever, particularly this graph represents the measurement from a single purified CNC. The cantilevers used in this study had maximum loads well under 10 nN averaging approximately 6.30 nN, therefore 3-point bending tests would not yield significantly different results from those performed on particles flat on the substrate. Therefore, the current method shown in Fig. 7(a-c) was able to produce valid and acceptable results on mechanical analysis. However, it is

important to note experimental limitations, specifically, contact cantilevers with a low stiffness and CNCs were tested on a flat surface. This low E_T could be connected to the use of a contact cantilever with a low stiffness of less than 10nN [48].

In addition, mechanical analysis of the purified and unpurified CNCs derived from hemp, revealed the correlation between the purification process and the mechanical properties. There are no statistically significant differences between any of the samples' E_T and maximum load, suggesting that the trace impurities have little impact on E_T (2.19 ± 0.15 GPa) and maximum load (6.29 ± 0.09 nN). This also suggests that the APS treatment is efficient in producing high quality CNCs from hemp waste. However, the purification played an important role in determining adhesion energy of the CNCs. Without purification, agglomerated CNCs had the lowest reported adhesion energy of 3.40E-17 J, which may be due to the impurities reducing the interaction between adjacent particles. This is further evidenced by the fact that the purified agglomerated CNC sample had the largest adhesion energy of 2.83E-16J. In summary, the purification after the APS treatment of hemp waste to produce clean CNCs played a major role in determining adhesion energy of hemp-derived CNCs, but a minor role in determining Young's modulus and maximum load of the hemp-derived CNCs.

2.5 Conclusion

CNCs were successfully extracted from HAW and then mechanically tested using AFM-FDS. FDS in an AFM was utilized on individual CNCs that were located on a flat glass surface as well as in larger agglomerations to investigate their mechanical properties. Mechanical properties were limited to Young's modulus, maximum load, and adhesion energy of four HAW-derived CNC samples; (i) unpurified agglomerated CNCs, (i) unpurified single CNCs, (iii) purified agglomerated CNCs, and (iv) purified single CNCs. All four samples of agglomerated

and single CNCs before and after purification were reported to have an average Young's modulus of 2.19 GPa and average maximum load of 6.3 nN, showing no statistically significant differences. The overall mechanical properties of CNC particles were not impacted whether they were located in agglomerations of particles or by how well they had been cleaned during extraction. However, statistically significant differences before and after purification in CNC extraction were found for adhesion energy measurements, suggesting that the adhesion energy on the surface of the CNCs are impacted which could be due to impurities coating the surface that might possibly mask the attractive forces of the CNCs to one another as well as other surfaces. Additionally, Young's modulus of the HAW-derived CNCs was on the low end of the range previously reported for the CNCs derived from other sources (cotton, tunicate, etc.) using different extraction methods. These results demonstrate that using AFM-FDS on CNCs located either directly on a flat surface or within agglomerated groups could be a potential approach for mechanical testing of small nanoparticles. Further research into the use of AFM-FDS on single and agglomerated CNCs using cantilevers with higher stiffness would be valuable for validating this approach of mechanical analysis. More thorough analysis of mechanical characteristics would increase our understanding of CNC mechanical behaviors and accommodate our ability to tune them with higher specificity, especially in the medical field. While impure residues from CNC extraction would want to be avoided, pure CNCs mechanical characteristics could be analyzed after adding them to biological media. Understanding how CNCs interact with different medias and how those medias impact CNCs adhesion capabilities could allow for more precise tuning. This potentially would enhance customization of medical applications and devices for things like cell attachment, drug delivery, and controlled disintegration of scaffolded implants.

Acknowledgements:

This work was supported by the Colorado Agricultural Experimental Station Grant (COL00408) and the student research grant funded by the American Association of Chemists and Colorists. The authors would like to acknowledge the ARC Materials and Molecular Analysis (MMA) at Colorado State University for providing equipment for material characterizations and specifically Dr. Bryan Newell for support on the XRD analysis.

Declarations

Ethical Approval

Not applicable

Funding

Colorado Agricultural Experimental Station Grant (COL00408)

American Association of Chemists and Colorists Student Research Grant

Availability of data and materials

The authors confirm that the data supporting the findings of this study are available within the article.

REFERENCES

(1) Delepierre, G.; Vanderfleet, O. M.; Niinivaara, E.; Zakani, B.; Cranston, E. D. Benchmarking Cellulose Nanocrystals Part II: New Industrially Produced Materials. *Langmuir* **2021**, *37* (28), 8393–8409. https://doi.org/10.1021/acs.langmuir.1c00550.

(2) Mali, P.; Sherje, A. P. Cellulose Nanocrystals: Fundamentals and Biomedical Applications. *Carbohydrate Polymers* **2022**, *275*, 118668. https://doi.org/10.1016/j.carbpol.2021.118668.

(3) George, J.; Sabapathi, S. Cellulose Nanocrystals: Synthesis, Functional Properties, and Applications. *Nanotechnology, Science and Applications* **2015**, *8*, 45–54. https://doi.org/10.2147/NSA.S64386.

(4) Vanderfleet, O. M.; Cranston, E. D. Production Routes to Tailor the Performance of Cellulose Nanocrystals. *Nat Rev Mater* **2020**, *6* (2), 124–144. https://doi.org/10.1038/s41578-020-00239-y.

(5) Jayanth, D.; Kumar, P. S.; Nayak, G. C.; Kumar, J. S.; Pal, S. K.; Rajasekar, R. A Review on Biodegradable Polymeric Materials Striving Towards the Attainment of Green Environment. *J Polym Environ* **2018**, *26* (2), 838–865. https://doi.org/10.1007/s10924-017-0985-6.

(6) Patil, T. V.; Patel, D. K.; Dutta, S. D.; Ganguly, K.; Santra, T. S.; Lim, K.-T. Nanocellulose, a Versatile Platform: From the Delivery of Active Molecules to Tissue Engineering Applications. *Bioactive Materials* **2022**, *9*, 566–589. https://doi.org/10.1016/j.bioactmat.2021.07.006.

(7) Punia Bangar, S.; Ilyas, R. A.; Chaudhary, N.; Dhull, S. B.; Chowdhury, A.; Lorenzo, J. M. Plant-Based Natural Fibers For Food Packaging: A Green Approach To The Reinforcement of Biopolymers. *J Polym Environ* **2023**, *31* (12), 5029–5049. https://doi.org/10.1007/s10924-023-02849-3.

(8) Azimi, B.; Sepahvand, S.; Ismaeilimoghadam, S.; Kargarzadeh, H.; Ashori, A.; Jonoobi, M.; Danti, S. Application of Cellulose-Based Materials as Water Purification Filters; A State-of-the-Art Review. *J Polym Environ* **2024**, *32* (1), 345–366. https://doi.org/10.1007/s10924-023-02989-6.

(9) Trache, D.; Hussin, M. H.; Haafiz, M. K. M.; Thakur, V. K. Recent Progress in Cellulose Nanocrystals: Sources and Production. *Nanoscale* **2017**, *9* (5), 1763–1786. https://doi.org/10.1039/C6NR09494E.

(10) Leung, A. C. W.; Hrapovic, S.; Lam, E.; Liu, Y.; Male, K. B.; Mahmoud, K. A.; Luong, J. H. T. Characteristics and Properties of Carboxylated Cellulose Nanocrystals Prepared from a Novel One-Step Procedure. *Small* **2011**, *7* (3), 302–305. https://doi.org/10.1002/smll.201001715.

(11) Cao, X.; Chen, Y.; Chang, P. R.; Stumborg, M.; Huneault, M. A. Green Composites Reinforced with Hemp Nanocrystals in Plasticized Starch. *J. Appl. Polym. Sci.* **2008**, *109* (6), 3804–3810. https://doi.org/10.1002/app.28418.

(12) Luzi, F.; Fortunati, E.; Puglia, D.; Lavorgna, M.; Santulli, C.; Kenny, J. M.; Torre, L. Optimized Extraction of Cellulose Nanocrystals from Pristine and Carded Hemp Fibres. *Industrial Crops and Products* **2014**, *56*, 175–186. https://doi.org/10.1016/j.indcrop.2014.03.006.

(13) Kassab, Z.; Abdellaoui, Y.; Salim, M. H.; Bouhfid, R.; Qaiss, A. E. K.; El Achaby, M. Micro- and Nano-Celluloses Derived from Hemp Stalks and Their Effect as Polymer

Reinforcing Materials. *Carbohydrate Polymers* **2020**, *245*, 116506. https://doi.org/10.1016/j.carbpol.2020.116506.
(14) Brinchi, L.; Cotana, F.; Fortunati, E.; Kenny, J. M. Production of Nanocrystalline Cellulose from Lignocellulosic Biomass: Technology and Applications. *Carbohydrate Polymers* **2013**, *94* (1), 154–169. https://doi.org/10.1016/j.carbpol.2013.01.033.
(15) Pacaphol, K.; Aht-Ong, D. Preparation of Hemp Nanofibers from Agricultural Waste by Mechanical Defibrillation in Water. *Journal of Cleaner Production* **2017**, *142*, 1283–1295. https://doi.org/10.1016/j.jclepro.2016.09.008.
(16) Novo, L. P.; Bras, J.; García, A.; Belgacem, N.; Curvelo, A. A. S. Subcritical Water: A Method for Green Production of Cellulose Nanocrystals. *ACS Sustainable Chem. Eng.* **2015**, *3* (11), 2839–2846. https://doi.org/10.1021/acssuschemeng.5b00762.
(17) Kang, X.; Kuga, S.; Wang, C.; Zhao, Y.; Wu, M.; Huang, Y. Green Preparation of Cellulose Nanocrystal and Its Application. *ACS Sustainable Chem. Eng.* **2018**, *6* (3), 2954–2960. https://doi.org/10.1021/acssuschemeng.7b02363.
(18) Wang, S.; Cheng, Q. A Novel Process to Isolate Fibrils from Cellulose Fibers by High-Intensity Ultrasonication, Part 1: Process Optimization. *Journal of Applied Polymer Science* **2009**, *113* (2), 1270–1275. https://doi.org/10.1002/app.30072.
(19) Man, Z.; Muhammad, N.; Sarwono, A.; Bustam, M. A.; Vignesh Kumar, M.; Rafiq, S. Preparation of Cellulose Nanocrystals Using an Ionic Liquid. *J Polym Environ* **2011**, *19* (3), 726–731. https://doi.org/10.1007/s10924-011-0323-3.
(20) Benhamou, K.; Dufresne, A.; Magnin, A.; Mortha, G.; Kaddami, H. Control of Size and Viscoelastic Properties of Nanofibrillated Cellulose from Palm Tree by Varying the TEMPO-Mediated Oxidation Time. *Carbohydrate Polymers* **2014**, *99*, 74–83. https://doi.org/10.1016/j.carbpol.2013.08.032.
(21) Novo, L. P.; Bras, J.; García, A.; Belgacem, N.; Curvelo, A. A. da S. A Study of the Production of Cellulose Nanocrystals through Subcritical Water Hydrolysis. *Industrial Crops and Products* **2016**, *93*, 88–95. https://doi.org/10.1016/j.indcrop.2016.01.012.
(22) Kargarzadeh, H.; Ioelovich, M.; Ahmad, I.; Thomas, S.; Dufresne, A. Methods for Extraction of Nanocellulose from Various Sources. In *Handbook of Nanocellulose and Cellulose Nanocomposites*; Kargarzadeh, H., Ahmad, I., Thomas, S., Dufresne, A., Eds.; Wiley-VCH Verlag GmbH & Co. KGaA: Weinheim, Germany, 2017; pp 1–49. https://doi.org/10.1002/9783527689972.ch1.
(23) Lam, E.; Leung, A. C. W.; Liu, Y.; Majid, E.; Hrapovic, S.; Male, K. B.; Luong, J. H. T. Green Strategy Guided by Raman Spectroscopy for the Synthesis of Ammonium Carboxylated Nanocrystalline Cellulose and the Recovery of Byproducts. *ACS Sustainable Chem. Eng.* **2013**, *1* (2), 278–283. https://doi.org/10.1021/sc3001367.
(24) Hu, Y.; Tang, L.; Lu, Q.; Wang, S.; Chen, X.; Huang, B. Preparation of Cellulose Nanocrystals and Carboxylated Cellulose Nanocrystals from Borer Powder of Bamboo. *Cellulose* **2014**, *21* (3), 1611–1618. https://doi.org/10.1007/s10570-014-0236-0.
(25) Castro-Guerrero, C. F.; Gray, D. G. Chiral Nematic Phase Formation by Aqueous Suspensions of Cellulose Nanocrystals Prepared by Oxidation with Ammonium Persulfate. *Cellulose* **2014**, *21* (4), 2567–2577. https://doi.org/10.1007/s10570-014-0308-1.
(26) Zhang, K.; Sun, P.; Liu, H.; Shang, S.; Song, J.; Wang, D. Extraction and Comparison of Carboxylated Cellulose Nanocrystals from Bleached Sugarcane Bagasse Pulp Using Two Different Oxidation Methods. *Carbohydrate Polymers* **2016**, *138*, 237–243. https://doi.org/10.1016/j.carbpol.2015.11.038.

(27) Jiang, H.; Wu, Y.; Han, B.; Zhang, Y. Effect of Oxidation Time on the Properties of Cellulose Nanocrystals from Hybrid Poplar Residues Using the Ammonium Persulfate. *Carbohydrate Polymers* **2017**, *174*, 291–298. https://doi.org/10.1016/j.carbpol.2017.06.080.
(28) Oun, A. A.; Rhim, J.-W. Isolation of Oxidized Nanocellulose from Rice Straw Using the Ammonium Persulfate Method. *Cellulose* **2018**, *25* (4), 2143–2149. https://doi.org/10.1007/s10570-018-1730-6.
(29) Bashar, M. M.; Zhu, H.; Yamamoto, S.; Mitsuishi, M. Highly Carboxylated and Crystalline Cellulose Nanocrystals from Jute Fiber by Facile Ammonium Persulfate Oxidation. *Cellulose* **2019**, *26* (6), 3671–3684. https://doi.org/10.1007/s10570-019-02363-7.
(30) Wang, H.; Pudukudy, M.; Ni, Y.; Zhi, Y.; Zhang, H.; Wang, Z.; Jia, Q.; Shan, S. Synthesis of Nanocrystalline Cellulose via Ammonium Persulfate-Assisted Swelling Followed by Oxidation and Their Chiral Self-Assembly. *Cellulose* **2020**, *27* (2), 657–676. https://doi.org/10.1007/s10570-019-02789-z.
(31) Liu, Y.; Liu, L.; Wang, K.; Zhang, H.; Yuan, Y.; Wei, H.; Wang, X.; Duan, Y.; Zhou, L.; Zhang, J. Modified Ammonium Persulfate Oxidations for Efficient Preparation of Carboxylated Cellulose Nanocrystals. *Carbohydrate Polymers* **2020**, *229*, 115572. https://doi.org/10.1016/j.carbpol.2019.115572.
(32) Filipova, I.; Serra, F.; Tarrés, Q.; Mutjé, P.; Delgado-Aguilar, M. Oxidative Treatments for Cellulose Nanofibers Production: A Comparative Study between TEMPO-Mediated and Ammonium Persulfate Oxidation. *Cellulose* **2020**, *27* (18), 10671–10688. https://doi.org/10.1007/s10570-020-03089-7.
(33) Khanjanzadeh, H.; Park, B.-D. Optimum Oxidation for Direct and Efficient Extraction of Carboxylated Cellulose Nanocrystals from Recycled MDF Fibers by Ammonium Persulfate. *Carbohydrate Polymers* **2021**, *251*, 117029. https://doi.org/10.1016/j.carbpol.2020.117029.
(34) Culsum, N. T. U.; Melinda, C.; Leman, I.; Wibowo, A.; Budhi, Y. W. Isolation and Characterization of Cellulose Nanocrystals (CNCs) from Industrial Denim Waste Using Ammonium Persulfate. *Materials Today Communications* **2021**, *26*, 101817. https://doi.org/10.1016/j.mtcomm.2020.101817.
(35) Marwanto, M.; Maulana, M. I.; Febrianto, F.; Wistara, N. J.; Nikmatin, S.; Masruchin, N.; Zaini, L. H.; Lee, S.-H.; Kim, N.-H. Effect of Oxidation Time on the Properties of Cellulose Nanocrystals Prepared from Balsa and Kapok Fibers Using Ammonium Persulfate. *Polymers* **2021**, *13* (11), 1894. https://doi.org/10.3390/polym13111894.
(36) Madani, H.; Wibowo, A.; Judawisastra, H.; Nishiyama, N.; Budhi, Y. W. One-Step Extraction of Cellulose Nanocrystals from High Lignin Biomass through Ammonium Persulfate Oxidation Method. *Adv. Nat. Sci: Nanosci. Nanotechnol.* **2022**, *13* (1), 015007. https://doi.org/10.1088/2043-6262/ac549a.
(37) Haunreiter, K. J.; Dichiara, A. B.; Gustafson, R. Nanocellulose by Ammonium Persulfate Oxidation: An Alternative to TEMPO-Mediated Oxidation. *ACS Sustainable Chem. Eng.* **2022**, *10* (12), 3882–3891. https://doi.org/10.1021/acssuschemeng.1c07814.
(38) Indirasetyo, N. L.; Kusmono. Isolation and Properties of Cellulose Nanocrystals Fabricated by Ammonium Persulfate Oxidation from Sansevieria Trifasciata Fibers. *Fibers* **2022**, *10* (7), 61. https://doi.org/10.3390/fib10070061.
(39) Çiçek Özkan, B.; Güner, M. Isolation, Characterization, and Comparison of Nanocrystalline Cellulose from Solid Wastes of Horse Chestnut and Chestnut Seed Shell. *Cellulose* **2022**, *29* (12), 6629–6644. https://doi.org/10.1007/s10570-022-04682-8.

(40) Habibi, Y.; Lucia, L. A.; Rojas, O. J. Cellulose Nanocrystals: Chemistry, Self-Assembly, and Applications. *Chem. Rev.* **2010**, *110* (6), 3479–3500. https://doi.org/10.1021/cr900339w.
(41) Sacui, I. A.; Nieuwendaal, R. C.; Burnett, D. J.; Stranick, S. J.; Jorfi, M.; Weder, C.; Foster, E. J.; Olsson, R. T.; Gilman, J. W. Comparison of the Properties of Cellulose Nanocrystals and Cellulose Nanofibrils Isolated from Bacteria, Tunicate, and Wood Processed Using Acid, Enzymatic, Mechanical, and Oxidative Methods. *ACS Appl. Mater. Interfaces* **2014**, *6* (9), 6127–6138. https://doi.org/10.1021/am500359f.
(42) Šturcová, A.; Davies, G. R.; Eichhorn, S. J. Elastic Modulus and Stress-Transfer Properties of Tunicate Cellulose Whiskers. *Biomacromolecules* **2005**, *6* (2), 1055–1061. https://doi.org/10.1021/bm049291k.
(43) Matsuo, M.; Sawatari, C.; Iwai, Y.; Ozaki, F. Effect of Orientation Distribution and Crystallinity on the Measurement by X-Ray Diffraction of the Crystal Lattice Moduli of Cellulose I and II. *Macromolecules* **1990**, *23* (13), 3266–3275. https://doi.org/10.1021/ma00215a012.
(44) Diddens, I.; Murphy, B.; Krisch, M.; Müller, M. Anisotropic Elastic Properties of Cellulose Measured Using Inelastic X-Ray Scattering. *Macromolecules* **2008**, *41* (24), 9755–9759. https://doi.org/10.1021/ma801796u.
(45) Hang, F.; Lu, D.; Bailey, R. J.; Jimenez-Palomar, I.; Stachewicz, U.; Cortes-Ballesteros, B.; Davies, M.; Zech, M.; Bödefeld, C.; Barber, A. H. *In Situ* Tensile Testing of Nanofibers by Combining Atomic Force Microscopy and Scanning Electron Microscopy. *Nanotechnology* **2011**, *22* (36), 365708. https://doi.org/10.1088/0957-4484/22/36/365708.
(46) Guhados, G.; Wan, W.; Hutter, J. L. Measurement of the Elastic Modulus of Single Bacterial Cellulose Fibers Using Atomic Force Microscopy. *Langmuir* **2005**, *21* (14), 6642–6646. https://doi.org/10.1021/la0504311.
(47) Iwamoto, S.; Kai, W.; Isogai, A.; Iwata, T. Elastic Modulus of Single Cellulose Microfibrils from Tunicate Measured by Atomic Force Microscopy. *Biomacromolecules* **2009**, *10* (9), 2571–2576. https://doi.org/10.1021/bm900520n.
(48) Cheng, Q.; Wang, S. A Method for Testing the Elastic Modulus of Single Cellulose Fibrils via Atomic Force Microscopy. *Composites Part A: Applied Science and Manufacturing* **2008**, *39* (12), 1838–1843. https://doi.org/10.1016/j.compositesa.2008.09.007.
(49) Tranchida, D.; Piccarolo, S.; Soliman, M. Nanoscale Mechanical Characterization of Polymers by AFM Nanoindentations: Critical Approach to the Elastic Characterization. *Macromolecules* **2006**, *39* (13), 4547–4556. https://doi.org/10.1021/ma052727j.
(50) Wagner, R.; Raman, A.; Moon, R. Transverse Elasticity of Cellulose Nanocrystals Via Atomic Force Microscopy. Tenth International Conference on Wood & Biofiber Plastic Composites and Cellulose Nanocomposites Symposium, May 11-13, Madison, WI. Madison, WI: Forest Products Society, c2010. ISBN 978-1-892529-55-8.
(51) Momeni, S.; Safder, M.; Khondoker, M. A. H.; Elias, A. L. Valorization of Hemp Hurds as Bio-Sourced Additives in PLA-Based Biocomposites. *Polymers* **2021**, *13* (21), 3786. https://doi.org/10.3390/polym13213786.
(52) El Achaby, M.; Kassab, Z.; Barakat, A.; Aboulkas, A. Alfa Fibers as Viable Sustainable Source for Cellulose Nanocrystals Extraction: Application for Improving the Tensile Properties of Biopolymer Nanocomposite Films. *Industrial Crops and Products* **2018**, *112*, 499–510. https://doi.org/10.1016/j.indcrop.2017.12.049.

(53) Jakubek, Z. J.; Chen, M.; Couillard, M.; Leng, T.; Liu, L.; Zou, S.; Baxa, U.; Clogston, J. D.; Hamad, W. Y.; Johnston, L. J. Characterization Challenges for a Cellulose Nanocrystal Reference Material: Dispersion and Particle Size Distributions. *J Nanopart Res* **2018**, *20* (4), 98. https://doi.org/10.1007/s11051-018-4194-6.
(54) Schütz, C.; Van Rie, J.; Eyley, S.; Gençer, A.; van Gorp, H.; Rosenfeldt, S.; Kang, K.; Thielemans, W. Effect of Source on the Properties and Behavior of Cellulose Nanocrystal Suspensions. *ACS Sustainable Chem. Eng.* **2018**, *6* (7), 8317–8324. https://doi.org/10.1021/acssuschemeng.8b00334.
(55) Ghodake, V. B.; Khare, R. A.; Mhaske, S. T. An Insight into Formation and Characterization of Nano-Cellulose Prepared From Industrial Cellulosic Wastes. *J Polym Environ* **2022**, *30* (1), 319–332. https://doi.org/10.1007/s10924-020-02026-w.
(56) Bhattacharjee, S. DLS and Zeta Potential – What They Are and What They Are Not? *Journal of Controlled Release* **2016**, *235*, 337–351. https://doi.org/10.1016/j.jconrel.2016.06.017.
(57) El Achaby, M.; Kassab, Z.; Aboulkas, A.; Gaillard, C.; Barakat, A. Reuse of Red Algae Waste for the Production of Cellulose Nanocrystals and Its Application in Polymer Nanocomposites. *International Journal of Biological Macromolecules* **2018**, *106*, 681–691. https://doi.org/10.1016/j.ijbiomac.2017.08.067.
(58) Yang, H.; Yan, R.; Chen, H.; Lee, D. H.; Zheng, C. Characteristics of Hemicellulose, Cellulose and Lignin Pyrolysis. *Fuel* **2007**, *86* (12–13), 1781–1788. https://doi.org/10.1016/j.fuel.2006.12.013.
(59) Abbasi Moud, A. Cellulose Nanocrystals Examined by Atomic Force Microscopy: Applications and Fundamentals. *ACS Food Sci. Technol.* **2022**, *2* (12), 1789–1818. https://doi.org/10.1021/acsfoodscitech.2c00289.
(60) Fortunati, E.; Puglia, D.; Monti, M.; Peponi, L.; Santulli, C.; Kenny, J. M.; Torre, L. Extraction of Cellulose Nanocrystals from Phormium Tenax Fibres. *J Polym Environ* **2013**, *21* (2), 319–328. https://doi.org/10.1007/s10924-012-0543-1.
(61) Lahiji, R. R.; Xu, X.; Reifenberger, R.; Raman, A.; Rudie, A.; Moon, R. J. Atomic Force Microscopy Characterization of Cellulose Nanocrystals. *Langmuir* **2010**, *26* (6), 4480–4488. https://doi.org/10.1021/la903111j.
(62) Hang, F.; Lu, D.; Bailey, R. J.; Jimenez-Palomar, I.; Stachewicz, U.; Cortes-Ballesteros, B.; Davies, M.; Zech, M.; Bödefeld, C.; Barber, A. H. *In Situ* Tensile Testing of Nanofibers by Combining Atomic Force Microscopy and Scanning Electron Microscopy. *Nanotechnology* **2011**, *22* (36), 365708. https://doi.org/10.1088/0957-4484/22/36/365708.
(63) Tan, E. P. S.; Lim, C. T. Mechanical Characterization of Nanofibers – A Review. *Composites Science and Technology* **2006**, *66* (9), 1102–1111. https://doi.org/10.1016/j.compscitech.2005.10.003.
(64) Zhao, Y.; Moser, C.; Lindström, M. E.; Henriksson, G.; Li, J. Cellulose Nanofibers from Softwood, Hardwood, and Tunicate: Preparation–Structure–Film Performance Interrelation. *ACS Appl. Mater. Interfaces* **2017**, *9* (15), 13508–13519. https://doi.org/10.1021/acsami.7b01738.

CHAPTER 3: EFFECTS OF AMMONIUM PERSULFATE OXIDATION REACTION TIME ON PERFORMANCE PROPERTIES OF CELLULOSE NANOCRYSTALS DERIVED FROM HEMP AGRO-WASTE

3.1 Summary

This study aimed to assess the effect of ammonium persulfate (APS) swelling and oxidation time on the characteristics of cellulose nanocrystals (CNCs) from hemp agro-waste (hurd). Specifically, this study focused on how varying reaction time impacted surface charge, size, chemical structure, mechanical characteristics, wettability, and cytotoxicity of the extracted CNCs. Increasing reaction time from 8 hours to 48 hours caused notable differences in size, chemical structure and wettability. Atomic force microscopy (AFM) analysis showed that length decreased from 467±277 nm to 159±67 nm and width decreased from 31.9±9.26 nm to 19.9±3.42 nm, with increasing reaction time from 8 hours to 48 hours, respectively. Fourier transform infrared spectroscopy (FTIR) evaluated the surface chemistry of CNCs and changes that occurred with increasing reaction times via the removal of hemicellulose and lignin as well as the addition of sodium carboxyl groups. Mechanical characteristic analysis using force distance spectroscopy (FDS) showed that reaction time does not have an impact on the intrinsic mechanical characteristics of CNCs, having a Young's modulus of around 73 GPa for all reaction times. CNCs were used to coat the surface of titanium (Ti) to study surface wettability, suggesting that reaction time has a noticeable impact on the CNCs hydrophilic nature of the treated Ti surface. Lastly, CNCs were not found to be cytotoxic, regardless of reaction time. Thus, controlling reaction time has the potential to aid in tuning CNCs to exhibit desirable characteristics for surface coating biomedical applications.

3.2 Introduction

Cellulose is the most abundant natural polymer in the world and is produced at a current estimate of over 10 metric tons per year[1]. It is composed of many glucose residues linked by β-1,4-glycosidic bonds creating a linear homopolymer. These glucose chains have amorphous and crystalline regions, where the crystalline regions can be separated from each other by removing the amorphous regions. Cellulose nanocrystals (CNCs) have been reported to range in diameter between 5-50 nm and lengths between 100-500 nm on average[2]. Other than being ubiquitous in nature, CNCs have unique properties such as large aspect ratios, high mechanical strength, biocompatibility, biodegradability, a modifiable surface, and natural hydrophilic nature. These properties allow for a wide range of potential applications for CNCs including: tissue engineering, tunable drug delivery and release, gene therapy, antimicrobial systems, and surface coating for medical devices/apparatuses[3,4]. Various mechanical and chemical methods have been used for the extraction of CNCs[5–8]. Chemical methods for CNC extraction are much more commonly used, with acid hydrolysis being one of the most common methods. However, over the last decade, ammonium persulfate (APS) oxidation has begun to grow in popularity[9–22].

APS oxidation has emerged in the last decade as a biofriendly method for CNC extraction[16]. When in solution, at room temperature, APS can be mixed gently with the starting plant waste material allowing for a swelling period. During this swelling period, APS is absorbed into the starting material prior to initiating oxidation and extraction of CNC. Application of heat catalyzes the reaction by decomposing peroxydisulfate ($S_2O_8^{2-}$) in a chain reaction into sulfate-free radicals that penetrate the amorphous region of the cellulose chain, effectively removing the amorphous regions and leaving the crystalline region in-tact. Furthermore, oxidation via the sulfate-free radical followed by peroxyl radical oxidation at the surface of the CNCs allows the

addition of carboxylic acid (COOH) groups[13]. APS oxidation is used for the direct extraction of carboxylated CNCs[12,13,16]. This method for CNC extraction has been used on various waste materials such as: recycled medium density fiberboard[15], jute fiber[9], industrial denim waste[11], poplar residues[23], balsa and kapok fibers[20], rice straw[21], and hemp agro-waste.

CNC characteristics vary depending on their source material and method of extraction. These differences include their size, morphology, crystallinity, thermal stability, surface properties, and cytotoxicity. APS, as previously discussed, add carboxyl groups to the surface of CNCs while acid hydrolysis adds sulfate groups to the surface of CNCs. Knowing that CNC properties vary, it begs the question, does varying different reaction conditions impact CNC properties. APS oxidation reaction time has become an area of interest by some research groups. These groups have looked into how reaction time impacts CNCs nanostructure, size, surface chemistry, crystal structure, thermal stability, and surface charge[9,11,13,20]. Being able to control CNC properties by slightly adjusting extraction conditions could allow for the development of specifically tuned nanoparticles.

Tuning CNCs for specific surface coating applications can be used to improve medical device and implant compatibility with the body[24]. Titanium (Ti) is one of the most common materials used for bone implants because of its corrosion resistance, hardness, and biocompatibility[23,25]. However, research is ongoing to reduce the body's natural immune response and improve the integration of Ti implants, for overall improvement in longevity of the devices[26]. Ti surfaces must be able to promote cell migration and attachment to increase long-term acceptance and integration with the body. Currently, there is a focus on modifying the surface of Ti with focus on things such as: micro-/macro-structure, wettability, cytocompatibility, mechanical strength matching, and antimicrobial effects[25–29].

The work reported hereby successfully demonstrates how varying reaction time of APS oxidation can impact the properties of CNCs extracted from hemp hurd. To date, no research groups have reported on how changing APS reaction time effects CNC mechanical characteristics, cytotoxicity, and hydrophilicity. The results of this study show that using CNCs as a coating material for Ti impacts the wettability of the surface in relation to reaction time, thus having potential to be tunable for different desirable applications. Specifically, varying reaction time has a noticeable impact on size and surface properties. Furthermore, this study highlights the effects, or lack thereof, that reaction time has on CNC mechanical properties and cytotoxicity.

3.3. Materials and Experiments

3.3.1 Materials

Raw Hemp (*Cannabis Sativa* L.) hurds, collected from HAW after fiber removal via retting and mechanical separation, were donated by a local hemp farm (Fort Collins, CO). The as received hemp hurds were processed using a mechanical blender (Cincred MC-BL618) into fine powder. Ammonium Persulfate (≥98%, Aldrich) was purchased from Sigma Aldrich and Sodium Hydroxide (99.4%, Fisher) purchased from Fisher Scientific. All chemicals used were of reagent grade and used without further purification.

3.3.2 Synthesis of CNC Nanoparticles

APS assisted swelling and oxidation was previously reported by Wang et. al [2020]. Hemp hurd was used as the starting material and ground down to make a fine HAW powder. 2 grams of raw HAW powder was added to 100 mL of 46% w/v (2 M) APS solution. The mixture mechanically stirred continually at 150 rpm for 3 hours to allow for adequate swelling. APS reaction was catalyzed by increasing the temperature to 60 °C and stirring speeds to 350 rpms.

Reactions were run for different time intervals: 8 hours (8-CNC), 12 hours (12-CNC), 16 hours (16-CNC), 20 hours (20-CNC), 24 hours (24-CNC), 36 hours (36-CNC), and 48 hours (48-CNC). The suspension was collected using a centrifuge at 6000 rpm for 15 minutes. Supernatant was decanted, distilled H_20 was then added to CNC tube and CNCs were resuspended using vortex machine till thoroughly mixed, and then centrifuged for 15 minutes. Wash cycles were performed 4 times or until pH 4 was reached. After washing, the product was then placed into 50 mL of distilled water and CNC/water suspension was brought to pH 7 using 1M NaOH added drop wise and was closely monitored using an electronic pH meter (OAKTON pH700). The suspension was put through a second round of wash/centrifuge cycles. After the final cleaning cycle, supernatant was decanted and remaining CNC product was kept in a wet state for further analysis. Seven samples, three batches per sample, were prepared for further analysis: (i) 8-CNC, (ii) 12-CNC, (iii) 16-CNC, (iv) 20-CNC, (v) 24-CNC, (vi) 36-CNC, and (vii) 48-CNC.

Samples for further analysis were prepared in two ways: (i) lyophilization was used to dry CNCs and (ii) aqueous suspensions made using wet CNCs. Wet CNCs were weighed and a 4% w/v aqueous suspension was initially prepared for all seven samples. Aqueous suspensions were vortexed for 10 minutes then underwent ultra-sonication (Fisher Scientific FB-505) in an ice-bath using a 1/8” probe (Fisher Scientific FB4418) at 30% of max amplitude (500 Watts at 6 kHz) for 12 minutes.

3.3.3 CNC percent yield

Lyophilization was performed on each CNC sample. Distilled water was added to the entire wet CNC sample until a total volume of 10 mL H_2O/CNC suspension was realized. CNCs were then dispersed in water using a vortex machine for 12-15 minutes. Ultra-sonication was performed on samples for 12 minutes. Samples were then frozen at -80 °C for 24 hours. Frozen

CNC were then dried using a lyophilizer (Labconco FreeZone 4.5 -50C Freeze Dryer Lyophilizer) for 24 hours, or until samples were completely dry. Percent yield was determined by using the final dried weight of the collected CNCs and dividing it by the percent content of cellulose in the HAW powder. The calculation was performed using equation 1:

$$\%yield = \frac{dry\ CNC\ weight\ (g)}{HAW\ powder \times \%cellulose\ content\ (g)} \times 100 \quad (1)$$

Momeni et al. reported hemp hurd to have a cellulose content of 40-48%[30]. For this research, 40% cellulose content will be used to determine the percent yield.

3.3.4 Fourier transform infrared spectroscopy (FTIR)

CNC chemical structure was evaluated using attenuated total reflectance-Fourier transform infrared spectroscopy (FTIR, Agilent Cary 630). FTIR spectra were recorded in 4000-650 cm^{-1} range with resolution of 2 cm^{-1} and an accumulation of 32 scans. CNC samples for analysis were prepared from lyophilized CNC product.

3.3.5 Dynamic Light Scattering (DLS) and Zeta Potential

The particle size and zeta potential of CNCs were analyzed (Malvern Instruments Zetasizer Nano ZS). DLS using a DTS0012 disposable cuvette was performed to assess the hydrodynamic radius of CNCs. Seven samples were prepared before measurements: (i) 8-CNC, (ii) 12-CNC, (iii) 16-CNC, (iv) 20-CNC, (v) 24-CNC, (vi) 36-CNC, and (vii) 48-CNC, by suspending CNCs in distilled water at room temperature at pH 7. Suspensions were diluted to concentrations of 0.0004% w/v. Tests on samples were run in sextuplicate. Mix-mode measurement phase analysis light scattering (M3-PALS) was performed using a DTS1070 disposable capillary cuvette for zeta potential measurements. An aqueous suspension for all

samples were prepared in distilled water at a concentration of 0.0004% w/v, pH 7, and at room temperature. Measurements for zeta potential were performed in sextuplicate.

3.3.6 Atomic Force Spectroscopy (AFM)

Seven CNC aqueous dispersions were used for this study: (i) 8-CNC, (ii) 12-CNC, (iii) 16-CNC, (iv) 20-CNC, (v) 24-CNC, (vi) 36-CNC, and (vii) 48-CNC. All samples were diluted to 0.04% w/v using the wet weight of CNC samples. 100 µL Poly-L-Lysine (PLL, 0.01% Thomas Scientific) was aliquoted onto mica (Ted Pella 50-20) surface and left to sit for 10 minutes. Mica was washed five times using distilled water and dried. 50 µL of 0.04% w/v CNC suspension was aliquoted onto PLL covered mica surface and spun for 25 seconds at 1000 rpms to evenly disperse CNCs. CNC covered mica samples were placed in desiccator and dried. Dry samples were scanned at room temperature using AFM (Park Systems XE-70). Contact cantilever (Park Systems CONTSCR) were used for imaging. Prior to imaging and CNC evaluation, XEI-70 was calibrated for accuracy. Images collected were used to analyze the length and width of samples using ImageJ for dimensional analysis of CNCs.

3.3.7 AFM – Force Distance Spectroscopy (FDS)

Mechanical characteristics for 8-CNC, 24-CNC, and 48-CNC samples were tested on the AFM using FDS (Park Systems XE-70). Each sample underwent mechanical testing using a contact cantilever (Park Systems NC-LC). One NC-LC cantilever was used for all three samples to have a more direct comparison between samples. NC-LC cantilevers have a cone shape tip with radius of ~20 nm and a spring force constant possessing nominal values of 100 N/m. Before FDS measurements were taken of the CNC samples, cantilever properties were set in XEI software as follows: Resonance frequency min = 300 kHz, max = 600 kHz, nominal = 450 kHz; Force-constant A-B sensitivity = 76.000 V/µm, force constant = 100 N/m; NCM amplitude gain

= 1.00 V/V. This step was done to verify that FDS measurements were consistent for all samples and ensure a direct comparison between mechanical properties. Individual CNCs were measured and a total of 50 measurements were performed for each sample, resulting in 50 CNCs tested per sample. During FDS the XEI software measured Young's modulus (E) and adhesion energy (J).

3.3.8 Wettability

Commercially available Titanium (Ti, 0.5 mm thick pure Titanium) was used to asses CNC wettability. Ti samples were cut into 4 cm^2 pieces and cleaned. The samples were soaked in acetone for 3 min and sonicated for 10 min to clean debris from the surface. The samples were further cleaned using diluted Micro 90 (International Products Corp.) cleaning solution and isopropanol followed by 10 min sonication in isopropanol first then deionized water (DI). The cleaned Ti samples were dried inside a desiccator prior to CNC coating. 1 mL of 4% w/v CNC aqueous suspension were aliquoted onto the Ti pieces, covering the entire surface. CNC coated Ti pieces were covered in a petri dish and placed in a desiccator until completely dry. Contact angle (CA) measurements were obtained using a Biolin Scientific Attension Theta Flex for all reaction time samples, as wells as pure Ti.

3.3.9 Cytotoxicity

Human adipose derived stem cell (ADSC) cell culture and cytotoxicity study was performed per method by Madruga et al. (2020). Human ADSCs isolated from adipose tissue and at passage three were obtained from Dr. Kimberly Cox-York's laboratory at Colorado State University. The protocol for ADSC isolation from healthy individuals was approved by Colorado State University Institutional Review Board. ADSC cells at passage 6 were cultivated in Dulbecco's Modified Eagle Medium (DMEM) supplemented with 10% fetal bovine serum and 1.0% penicillin/streptomycin and maintained at 37 C and 5% CO_2. 48-micro well plate was

seeded with ADSCs 20,000 cells/mL concentration for 24 hours. During the culture period, CNCs were prepared using dried CNC material. 1mg/mL of CNCs were soaked in growth media (MEM Alpha Modification, HyCloneTM) (CNC/MEM) for 12 hours prior to being dispersed via ultra-sonication for 10 minutes. CNC/MEM samples were placed in hot water bath prior to use, during which time growth media was removed from seeded cell wells. Using a syringe and 0.22 nylon syringe filter (Fisher Scientific 03-253-901), 100 µL of CNC/MEM suspension was added to seeded cell wells. LDH assay was performed after 1 day of culture to evaluate the toxicity of CNC samples toward the cells. After 24 h of cell culture in media containing CNC samples, 50 µL of media with the samples was added to an equal amount of LDH (QuantichromBio Assay Systems) in a 96 well plate, followed by an incubation time of 30 min. The absorbance of the solution in each well was measured at 490 nm and 680 nm (n = 5) using a plate reader (BMG LABTECH FLUOstarOmega) [31].

3.3.10 Statistical Analysis

Statistical analysis was conducted for size, mechanical properties, wettability, and cytotoxicity. Two-way ANOVA and Tukey multiple range tests were performed using Rstudio statistical software. Analysis and comparisons of all CNC reaction times were made.

3.4 Results and discussion

3.4.1 CNC dispersion and colloidal stability

This study assesses the impact that reaction time has on CNC properties. For medical applications, it would be beneficial to be able to account for specific changes to CNCs by modulating various extraction parameters. CNCs were extracted from hemp waste via APS assisted swelling followed by oxidation[22] for varying reaction times. The use of APS adds a carboxyl group to the surface of CNCs, creating a net negative charge at the surface of the

nanoparticle. Zeta potential measured using M3-PALS was used to determine the surface charge, and by extension the stability of the CNC particles. Charges lower than -25 mV are reported to be colloidally stable in a suspension[20]. CNCs at all reaction times were found to have zeta potential lower than -25 mV (Fig. 1i). The mean and standard deviation for all CNC reaction times are shown in Table 1. Other research groups that have also used APS oxidation reported zeta potentials between -30 mV and -40 mV[9,22], which are in good agreement with the values reported in this study.

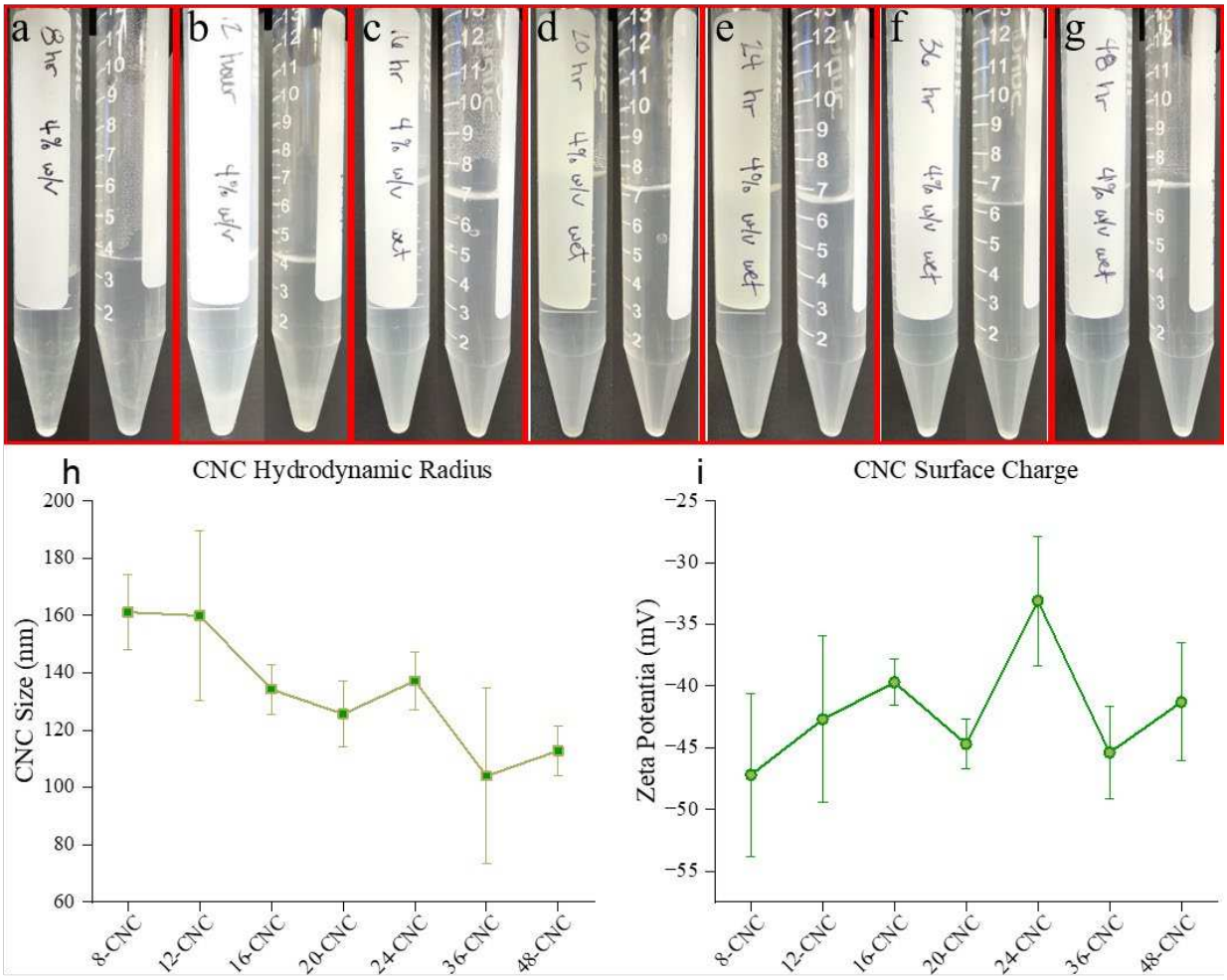

Figure 3.1*: 4% w/v CNC aqueous dispersions (top row), DLS hydrodynamic radius (h), and Zeta potential of 8-CNC (a), 12-CNC (b), 16-CNC (c), 20-CNC (d), 24-CNC (e), 36-CNC (f), and 48-CNC (g).*

To highlight the colloidal stability of our samples, 4% w/v CNC aqueous suspension were made and left for up to 3 months. 36-CNC and 48-CNC were the most transparent aqueous suspensions, while 8-CNC and 12-CNC were the opaquest. This trend of decreasing opacity with respect to increasing reaction time was previously reported[20]. 8-CNC and 12-CNC (Fig. 1 a and b) had visible aggregates in the aqueous suspension, thus implying that they were not colloidally stable. 16-CNC, 20-CNC, 24-CNC, 36-CNC, and 48-CNC (Fig. 1 c, d, e, f, and g respectively) aqueous dispersions were homogeneous and absent of any visible aggregates, suggesting that they were colloidally stabile. Interestingly, while the zeta potential for all samples reported surface charges well below -25 mV with 8-CNC reporting the lowest surface charge of -47 mV, the aqueous suspensions of 8-CNC and 12-CNC began to aggregate and settle after sitting for 3 months. Due to the change in opacity of the samples with reaction time, we decided use DLS to quickly asses if there were changes in particle size. As reaction time increased, the hydrodynamic radius of the samples shown in Fig. 1h and table 1, suggesting an overall trend relating reaction time to CNC size (Fig. 1h). Of note, this relationship between opacity and CNC size raises the question if size impacts opacity. This study, however, will not be assessing the potential relationship between CNC size and aqueous suspension opacity.

3.4.2 Size and morphology

Upon further investigation into the impact of CNC properties with reaction time, % yield and CNC size were assessed. Fig. 2 shows lyophilized CNCs for all reaction times. As reaction time increased the color of the CNCs changes from a tanish color to a very white color (Fig. 2 a-g). Also, the amount of CNCs seemed to decrease with increased reaction time; 8-CNC, 12-CNC, 16-CNC, 20-CNC, 24-CNC, 36-CNC, and 48-CNC dry weights were 709, 412, 294, 188, 270, 200, and 22 mg, respectively (Table 1). Percent yield was found by taking the dried CNC weight

and using equation 1 reported in the methods section, with values as follows: 88.6%, 51.5%, 36.8%, 23.5%, 33.8%, 25%, and 2.76% for 8-CNC, 12-CNC, 16-CNC, 20-CNC, 24-CNC, 36-CNC, and 48-CNC, respectively.

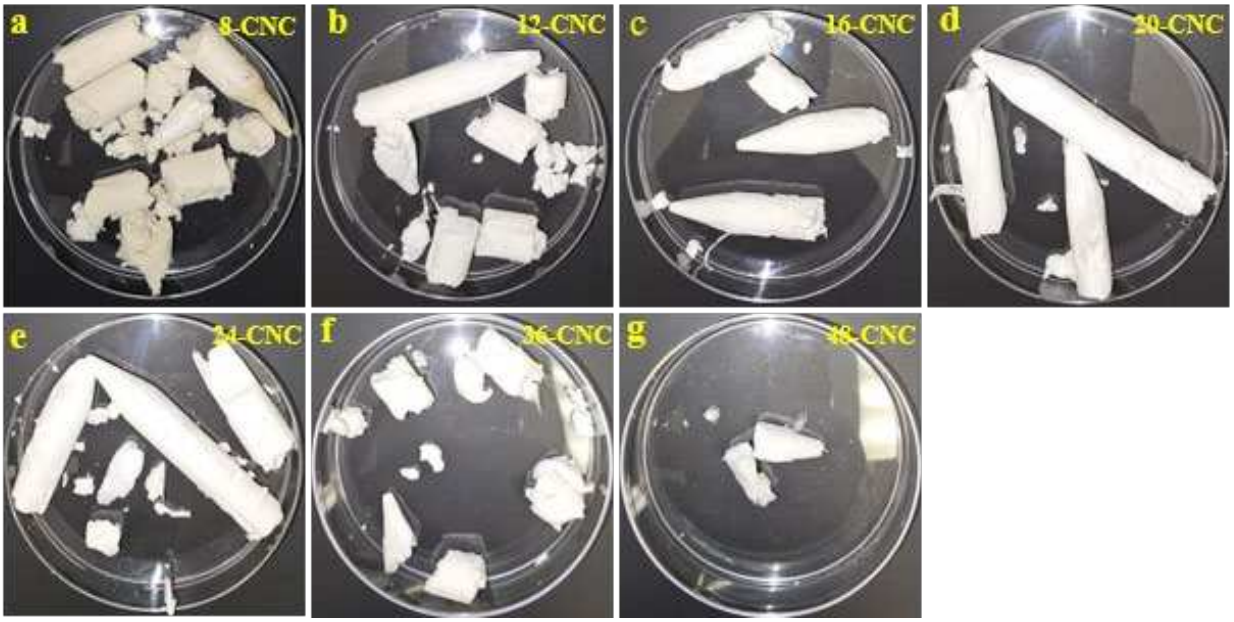

Figure 3.2*: Dried CNC samples: 8-CNC (a), 12-CNC (b), 16-CNC (c), 20-CNC (d), 24-CNC (e), 36-CNC (f), and 48-CNC (g).*

Bashar et al. reported CNC yields of 64%, 61%, 57%, and 54% for reaction times of 6 h, 8 h, 12 h, 16 h, and 24 h, respectively, from Jute fiber using APS oxidation[9]. Our results align with these previeously reported results, implying a potential relationship between reaction time and final product yield.

AFM images of all CNC samples were taken using a CONTSCR cantilever. This cantilever was chosen due to its tip being <10 nm. This is important because convolution of the tip shape in conjunction with the sharp edges of the nanocrystals can make the width of the CNCs appear to be larger than they truly are[32]. While this phenomenon is relevant, for our purpose to assess potential changes in CNC samples size with respect to reaction time, it was acceptable to perform size comparisons using this method. Thus, using a cantilever with a

significantly small tip, such as a CONTSCR, was desirable for imaging and comparing CNC sizes. Fig. 2 row 2 show AFM force images taken with the CONTSCR. At all reaction times, the CNCs appear to have a similar needle-like shape morphology, which is in good agreement with previous reports[32,33]. Taking note of the scale bars for 8-CNC and 12-CNC in Fig. 3a and 3b, respectively, they are 1000 nm while the scale bars for the remaining samples are 500 nm (Fig. 3c-g). With this information it is more pronounce that the decrease in size and dispersion of particles is related to increases in reaction time. As reaction time increases CNCs seem to be able to separate more effectively, as well as become smaller and more uniform in size. 8-CNC had very large CNC particles that were closer together, with noticeable overlap in some areas (Fig. 3a). This difficulty separating these CNCs was also evidenced in the 4% aqueous suspension shown in Fig. 1a, with the aggregation of particles.

Sample size distributions for length and width are shown by the graphs in Fig. 3 h and i, respectively. The mean and standard deviation for all samples is located on tables shown in Fig. 2h and i, as well as in Table 1. Looking at the CNC size distributions, 8-CNC had the largest distribution as well as the largest mean value for both length and width with values of 467 ± 277 nm and 31.9 ± 9.26 nm, respectively. As reaction time increased CNC size showed large statistically significant differences for both length and width between 8- , 24- , and 48-CNC reaction times. However, there were no significant differences between 12-, 16- , and 20-CNC or between 20- , 24-, and 36-CNC reaction times. 48-CNC nanoparticles were the smallest, with a length and width of 159 ± 63 nm and 19.9 ± 3.42 nm, respectively. The aspect ratio for 8-CNC, 12-CNC, 16-CNC- 20-CNC, 24-CNC, 36-CNC and 48-CNC were 14.9 ± 8.54, 10.8 ± 4.21, 10.4 ± 5.24, 8.30 ± 2.91, 9.47 ± 5.30, 9.56 ± 5.18, and 8.06 ± 3.09, respectively. Overall, it appears that aspect ratio decreases with increasing reaction time, with a few noticeable deviations from

the trend. Of note, as reaction time increased, not only did the size of the CNCs decrease, the distribution also narrowed (Fig. 3h and i), indicating that the particles became more uniform and consistent in size.

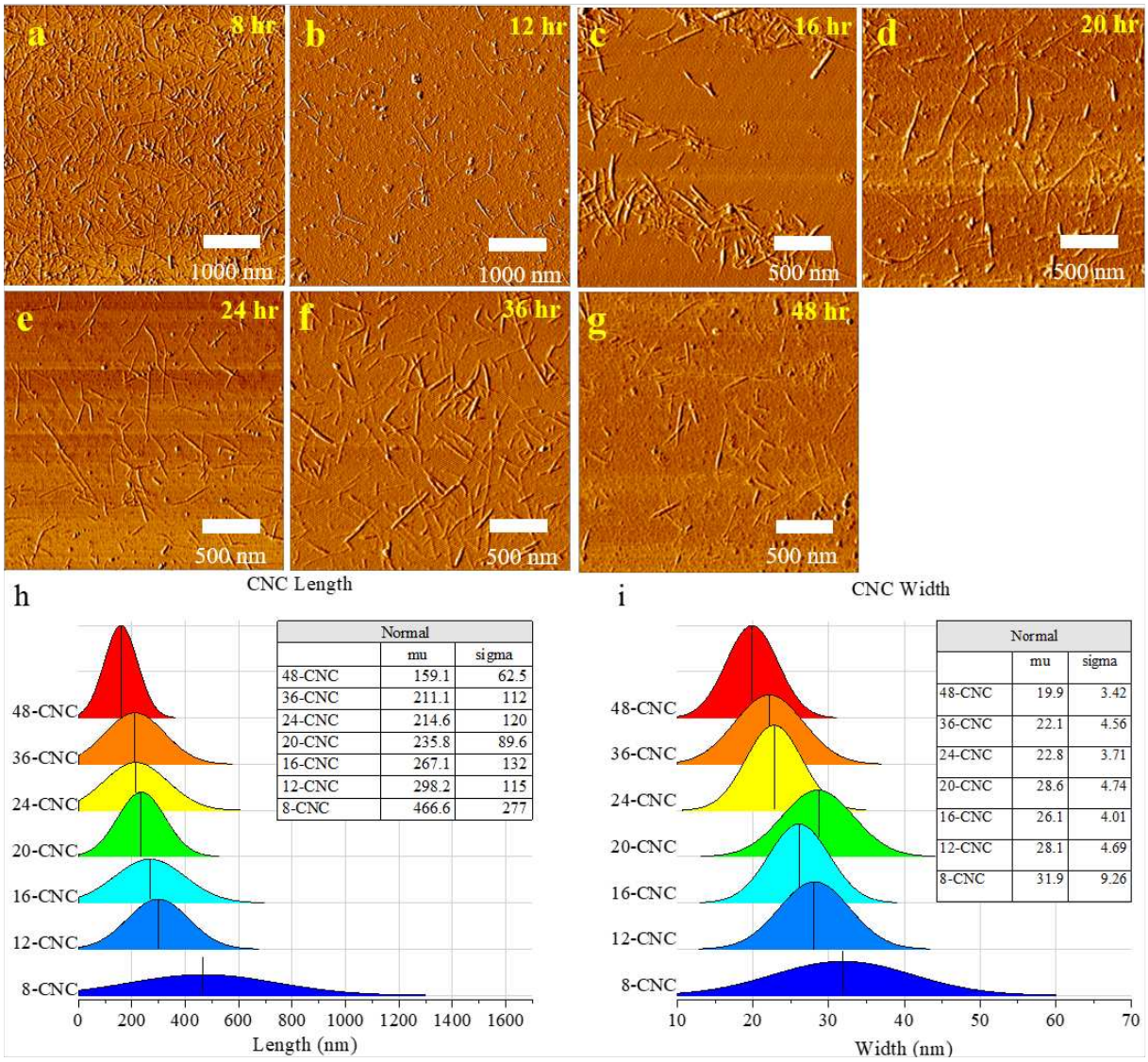

Normal	mu	sigma
48-CNC	159.1	62.5
36-CNC	211.1	112
24-CNC	214.6	120
20-CNC	235.8	89.6
16-CNC	267.1	132
12-CNC	298.2	115
8-CNC	466.6	277

Normal	mu	sigma
48-CNC	19.9	3.42
36-CNC	22.1	4.56
24-CNC	22.8	3.71
20-CNC	28.6	4.74
16-CNC	26.1	4.01
12-CNC	28.1	4.69
8-CNC	31.9	9.26

Figure 3.3*: AFM images (first and second rows), length distribution (h), and width distribution (i) of 8-CNC (a), 12-CNC (b), 16-CNC (c), 20-CNC (d), 24-CNC (e), 36-CNC (f), and 48-CNC (g).*

All of this implies that reaction time has a strong effect on CNC extraction, effecting %yield, size, and colloidal stability.

Tabel 3.1: CNC Size and Surface Properties

Reaction Time (hours)	DLS hydrodynamic radius (nm)	Zeta Potential (mV)	CNC Dry Weight (mg)	CNC yield (%)	CNC Length (nm)	CNC Width (nm)	Aspect Ratio
8 hr	161 ± 13	-47.2 ± 6.6	709	88.6	467 ± 277	31.9 ± 9.26	14.9 ± 8.54
12 hr	160 ± 30	-42.7 ± 6.8	412	51.5	298 ± 115	28.1 ± 4.69	10.8 ± 4.21
16 hr	134 ± 8.6	-39.7 ± 1.9	294	36.8	257 ± 132	26.1 ± 4.01	10.4 ± 5.24
20 hr	126 ± 12	-44.9 ± 2.0	188	23.5	236 ± 90	28.6 ± 4.74	8.30 ± 2.91
24 hr	137 ± 10	-33.1 ± 5.2	270	33.8	215 ± 120	22.8 ± 3.71	9.47 ± 5.30
36 hr	103 ± 31	-45.4 ± 3.7	200	25	211 ± 112	22.1 ± 4.56	9.56 ± 5.18
48 hr	113 ± 9	-41.3 ± 4.8	22	2.76	159 ± 63	19.9 ± 3.42	8.06 ± 3.09

A direct comparison of chemical structure between sample reaction times was performed. Cellulose, in plants, are accompanied by other cellulosic material, such as lignin and hemicellulose[34–36], prior to extraction. Furthermore, it has been documented that APS oxidation attaches carboxyl groups to the surface of CNCs during extraction[18,37,38]. 8-CNC, 12-CNC, 16-CNC, 20-CNC, 24-CNC, 36-CNC, and 48-CNC samples were characterized via their chemical composition and surface functionality using FTIR spectra, shown in Fig. 4. All samples showed characteristic cellulose peaks at 3340 cm^{-1} and 2890 cm^{-1} which correlate with the stretching vibration of -OH and CH- groups[20,33], respectively. 8-CNC has a noticeable peak at 1734 cm^{-1} and 1238 cm^{-1} (Fig. 4) which are typically associated with lignin[39] and hemicellulose[40], respectively. It should also be noted, that while the intensity of each of these peaks is greatly reduce, they are still present for 12-CNC. These peaks do not show on any other sample, suggesting that lignin and hemicellulose are completely removed by 16 hours reaction time.

3.4.3 FTIR analysis

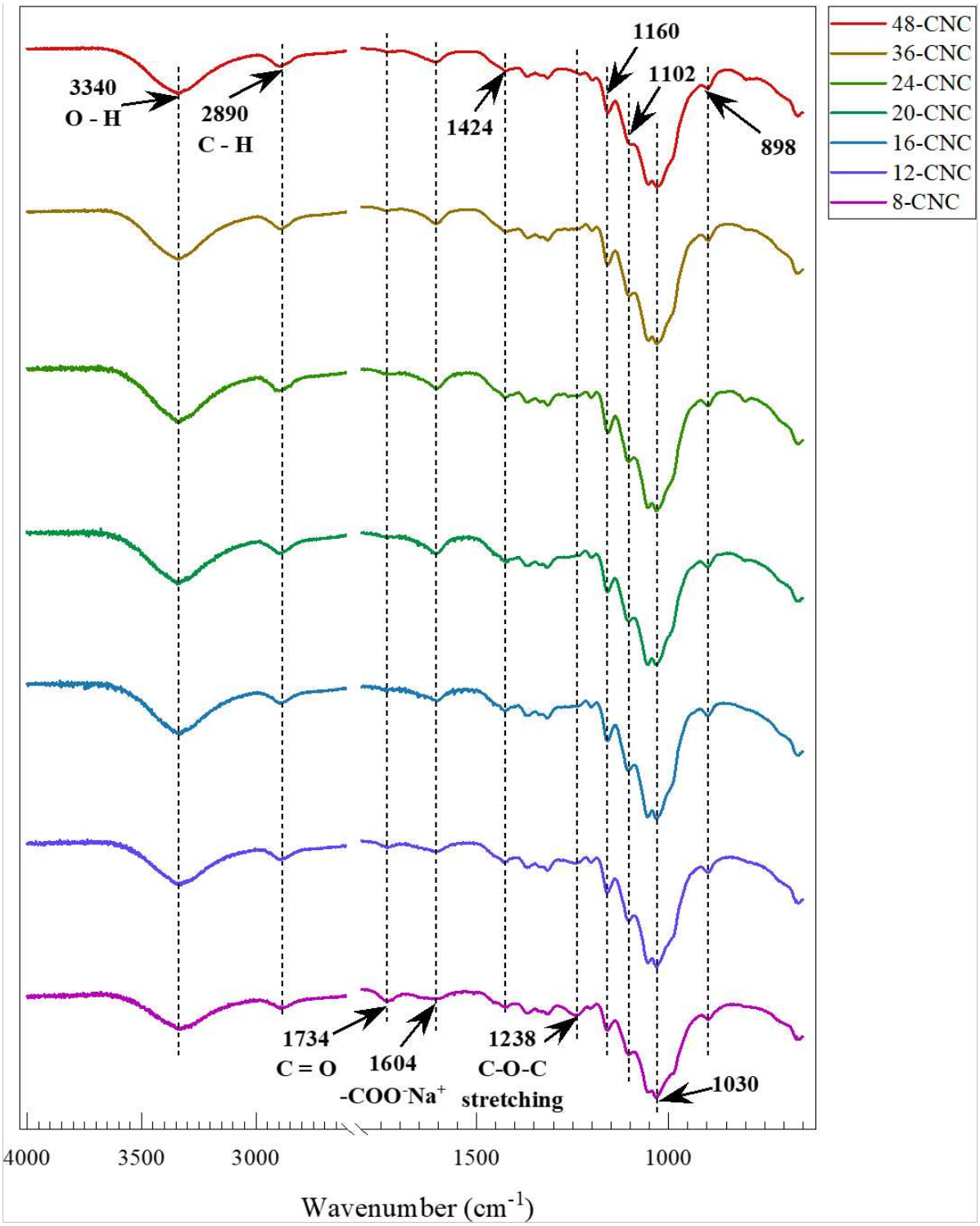

Figure 3.4*: FTIR spectra of hemp extracted CNCs at different reation times: 8-CNC, 12-CNC, 16-CNC, 20-CNC, 24-CNC, 36-CNC, and 48-CNC.*

It appears that there is a peak at 1604 cm^{-1}, which is indicative of the presence of sodium carboxylate ($-COOH^{-}NA^{+}$)[15,16,38] as early as 8-CNC, and this peak increases with intensity as the reaction time goes to 24 hours (Fig. 4). Interestingly, the peak at 1604 cm^{-1} seems to have the greatest intensity at 24-CNC and there is a decrease in intensity reaction time increases to 48 hours. Thus, lignin and hemicellulose are fully removed after 12-CNC and sodium carboxylate seems to be present for all reactions. These results suggest that the only chemical change to the CNC are at the surface. This can be inferred by looking at all other characteristic peaks, 3340 cm^{-1}, 2890 cm^{-1}, 1424 cm^{-1}, 1160 cm^{-1}, 1102 cm^{-1}, 1030 cm^{-1}, and 898 cm^{-1}, and their lack of any significant changes in intensity.

3.4.4 CNC mechanical properties

FDS using AFM was used to study the mechanical properties of individual hemp-derived CNCs for different APS oxidation reaction times. Previous studies have shown the use of FDS as a viable method to measure CNC mechanical properties on a flat surface[41]. In our previous study we illustrated how FDS can be used on single or agglomerated CNCs, and that there was no significant difference in the mechanical characteristics between these groups. Furthermore, we also showed that impurities do not impact the young's modulus (E_T) of CNCs. This is important since there is evidence that lignin and hemicellulose may still be present on 8-CNC and 12-CNC samples (Fig. 4). Therefore, during this study we measured the young's modulus and adhesion energy of 50 individual CNCs per group, whether they were aggregated or separate from other surrounding CNCs. Some of other results during this study indicate that the samples that show the greatest differences are between 8-CNC, 24-CNC, and 48-CNC. Specifically, there was a notable difference in size and chemical characteristics between these samples. Moving forward

we chose to perform a mechanical study on only 8-CNC, 24-CNC, and 48-CNC for the previously mentioned reasons.

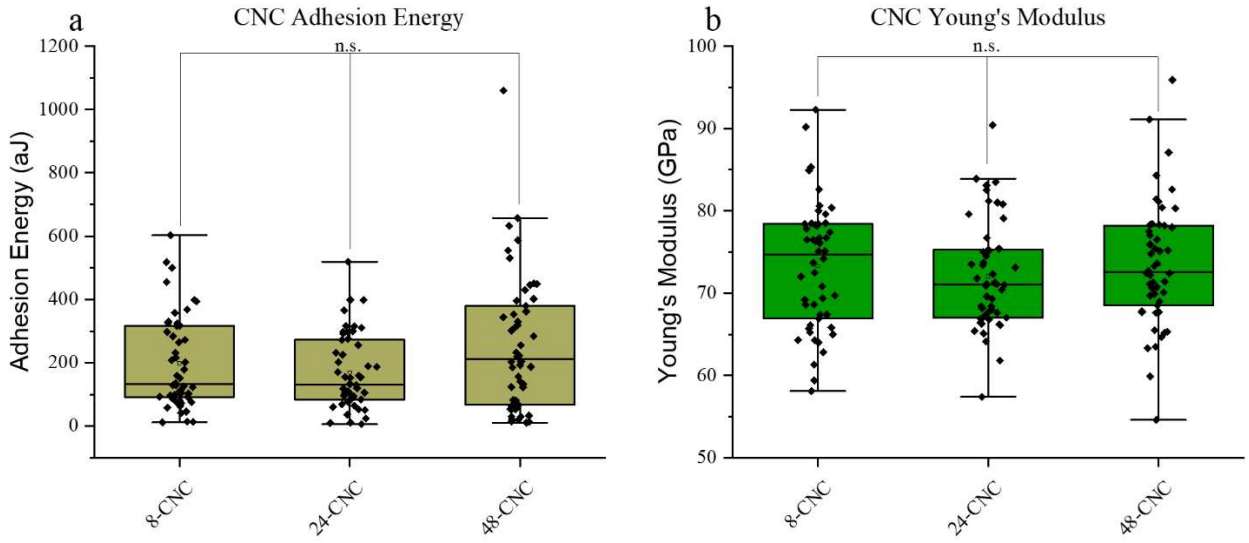

Figure 3.5*: AFM-FDS adhesion energy (a) and Young's modulus (b) of 8CNC, 24-CNC, and 48-CNC.*

The adhesion energy and E_T are shown in Fig. 5a and Fig. 5b, respectively. Adhesion energy reports how hard it was for the cantilever to lift off the sample. This measurement can give an insight into how well a material is able to adhere to another surface. 8-CNC, 24-CNC, and 48-CNC had adhesion energies of 198 ± 145 aJ, 170 ± 118 aJ, and 256 ± 215 aJ, respectively (Fig. 5a and Table 2). 48-CNC had a larger mean, which could imply that these CNCs may have had a slightly more attractive force at their surface than the other samples. However, statistical analysis showed that there was no significant difference between these samples. Thus, more analysis would need to be performed to test if there is a difference in attractive forces between the samples.

Wagner et al. reported the E_T of tunicate derived CNCs, using acid hydrolysis, to be between 2 and 37 GPa[41]. Multiple sources have reported the axial elastic modulus (E_A) of wood and tunicate derived CNCs, using acid hydrolysis, to be between 110 and 200 GPa. We

previously reported E_T values of ~ 2 GPa for hemp derived CNCs, using APS oxidation, via a CONTSC cantilever (0.2 N/m). For this investigation, however, an NC-LC cantilever was chosen to perform these measurements due to it having a higher stiffness (100 N/m). It was also important that all measurements performed used the same NC-LC cantilever. This was done to ensure that potential differences in cantilevers did not influence our measurements causing erroneous differences between groups that did not truly reflect the impact of APS reaction time alone. 8-CNC, 24-CNC, and 48-CNC had E_T values of 73.3 ± 7.69 GPa, 72.0 ± 6.58 GPa, and 73.5 ± 7.63 GPa, respectively (Fig. 5b and Table 2). These values are larger than what Wagner et al. reported, and smaller than what other research groups have reported. However, what is of most importance to us is how reaction time may have caused potential differences in E_T. Statistical analysis of these results show that there is no statistically significant difference in the mechanical characteristics of these CNCs due to reaction time.

Table 3.2: CNC Mechanical Properties

Reaction Time (hours)	Young's Modulus (GPa)	Adhesion Energy (aJ)
8 hr	73.3 ± 7.69	198 ± 145
24 hr	72.0 ± 6.58	170 ± 118
48 hr	73.5 ± 7.63	256 ± 215

3.4.5 Surface wettability

CA is the angle at which water that is in contact with a surface makes at the edges of the droplet and is a common method used to determine the wettability of a material[42], such as Ti. Ti has become a commonly used material for implants[43] due to its superior biocompatible, which is determined by it surface properties[23]. One of those important surface properties is the hydrophilicity at the location of contact between living tissue and Ti. Using Ti as a base material, we assessed how our samples impacted the its surface wettability to see if there is a relationship between reaction time and CNC hydrophilicity. Fig. 6 rows 1 and 2 show pictures of titanium

coated with our samples. 8-CNC behaved in the most unique way (Fig. 6a) by forming a film that pealed away from the surface of the Ti.

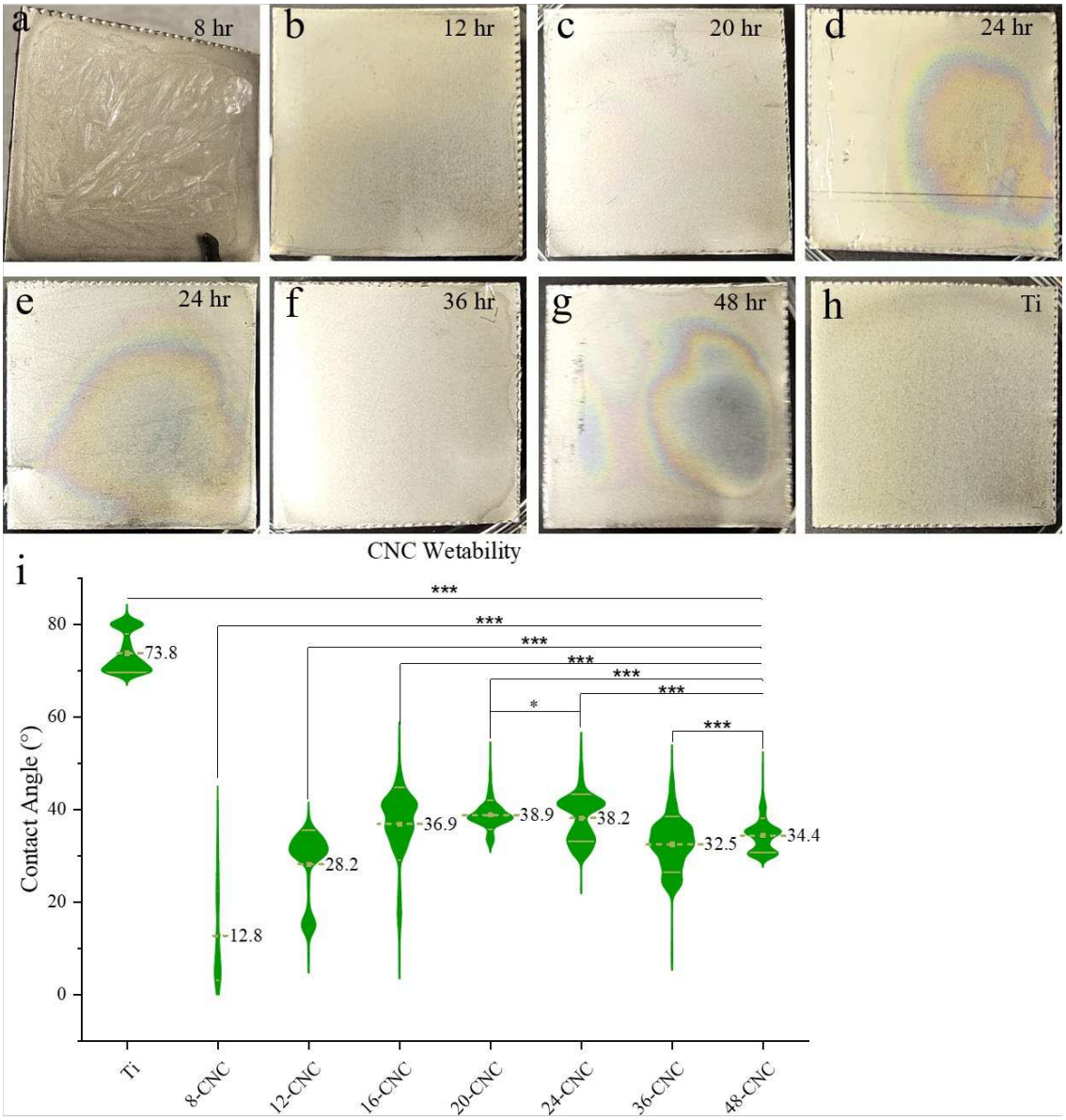

Figure 3.6*: Titanium coated with CNCs (row 1 and 2) and surface wettability (i) of 8-CNC (a), 12-CNC (b), 16-CNC (c), 20-CNC (d), 24-CNC (e), 36-CNC (f), 48-CNC (g), and pure Titanium (h). Statistical significances (p-value) were represented as * $p \leq 0.05$ and *** $p \leq 0.0001$.*

This can be seen by how different the texture of 8-CNC is compared to all other samples (Fig. 6 a-h). All other samples appeared to have a more secure attachment to the Ti surface, but further research would be required to determine attachment properties.Interestingly, as can be seen in

Fig. 6d, e, g, and to a smaller degree Fig. 6c, there is a rainbow effect. This has to do with the chiral nature of CNCs[44] and the angle the light was hitting the surface of the samples[22]. Even though it cannot be seen in the images, all samples showed this chiral nature when you rotated the samples at different degrees in the light. While this phenomenon was interesting, no research was performed at this time to see if the chiral nature of CNCs had any relationship to the hydrophilic nature of the CNCs.

Fig. 6i is a violin plot showing the CA of water with the surface of the samples. This plot was chosen to give a better understanding as to how the contact angle behaved with time. First, we measured a pristine Ti sample (Fig. 6h) to use as our control. At all times, the contact angle remained below 90°, suggesting that Ti has a natural hydrophilic nature[42], with a mean value of 73.8°. All treated surfaces exhibited a significantly reduced CA compared to pure Ti, implying that coating Ti with CNCs improves the hydrophilic nature of the surface. 8-CNC had the lowest average CA value of 12.8°, however the distribution of measured angles is very spread out. This has to do with the fact that the water quickly spread out over the surface after being dropped onto the sample. Zhang et al. reported on hemicellulose, stating that it has a hydrophilic nature[45]. This could potentially have something to do with the surface topography. 8-CNC has an obvious topography that is completely different from all other samples, and the film separating from the Ti surface could have played a role in the hydrophilicity of the sample. Furthermore, taking into account the FTIR results (Fig. 4) in conjunction with the extremely low CA of 8-CNC (Fig. 6a), it seems possible that hemicellulose is still present and has increased the hydrophilicity of this sample. This is further evidences when looking at 12-CNC (Fig. 6i), whose CA has a mean value of 28.2°, and that this sample also shows evidence of containing hemicellulose (Fig. 4). 20-CNC has the most stable CA distribution of all the samples, as well as the largest mean value of 38.9°

(Fig. 6i). This may suggest that at this point all hemicellulose has bee successfully removed from the samples. With increasing reaction time above 20 hours, the CA starts to drop back down. It may be, that after the complete removal of hemicellulose the size of the CNCs themselves start to play a larger role in the hydrophilic nature of the surface of Ti. Further research would be required to verify if the size of CNC particles plays a direct role in the hydrophilicity of the Ti surface. Statistical analysis was performed, comparing all samples with one another, and it was found that all samples had a statistically significant difference from one another. Suggesting the potential to control surface wettability by adjusting APS reaction time.

3.4.6 CNC cytotoxicity

For this study, CNCs at a concentration of 1 mg/mL were suspended in MEM growth media, that was used to culture ADSCs, for 24 hours. Using LDH analysis, the cytotoxicity of the CNCs were estimated in order to evaluate the number of cells that would lyse or die in the culture media containing our filtered CNCs. Upon cell damage, cell plasma membranes will lyse, releasing the LDH enzyme into the surround media. In order to determine the cytotoxicity a control sample was prepared that would undergo normal cell growth and death in MEM, providing a spontaneous release of LDH from ADSCs in a healthy environment. Following CyQuant LDH Cytotoxicity Assay Kit protocol, another control group was made that had a lysing agent, Triton, added to the growth media in order to ensure maximum cell death/membrane lysis[31,46]. Fig. 7 shows the LDH release measured for both controls (control and Triton) and all 7 CNC samples (8-CNC, 12-CNC, 16-CNC, 20-CNC, 24-CNC, 36-CNC, and 48-CNC). Our samples had a much lower release of LDH compared to Triton, and the LDH values were statistically similar to the positive control sample. Thus, implying that all our samples, when introduced to ADSCs, were not cytotoxic. Of note, further analysis by coating a surface,

such as Ti, with our samples and introducing cells would need to be performed to confirm the above results.

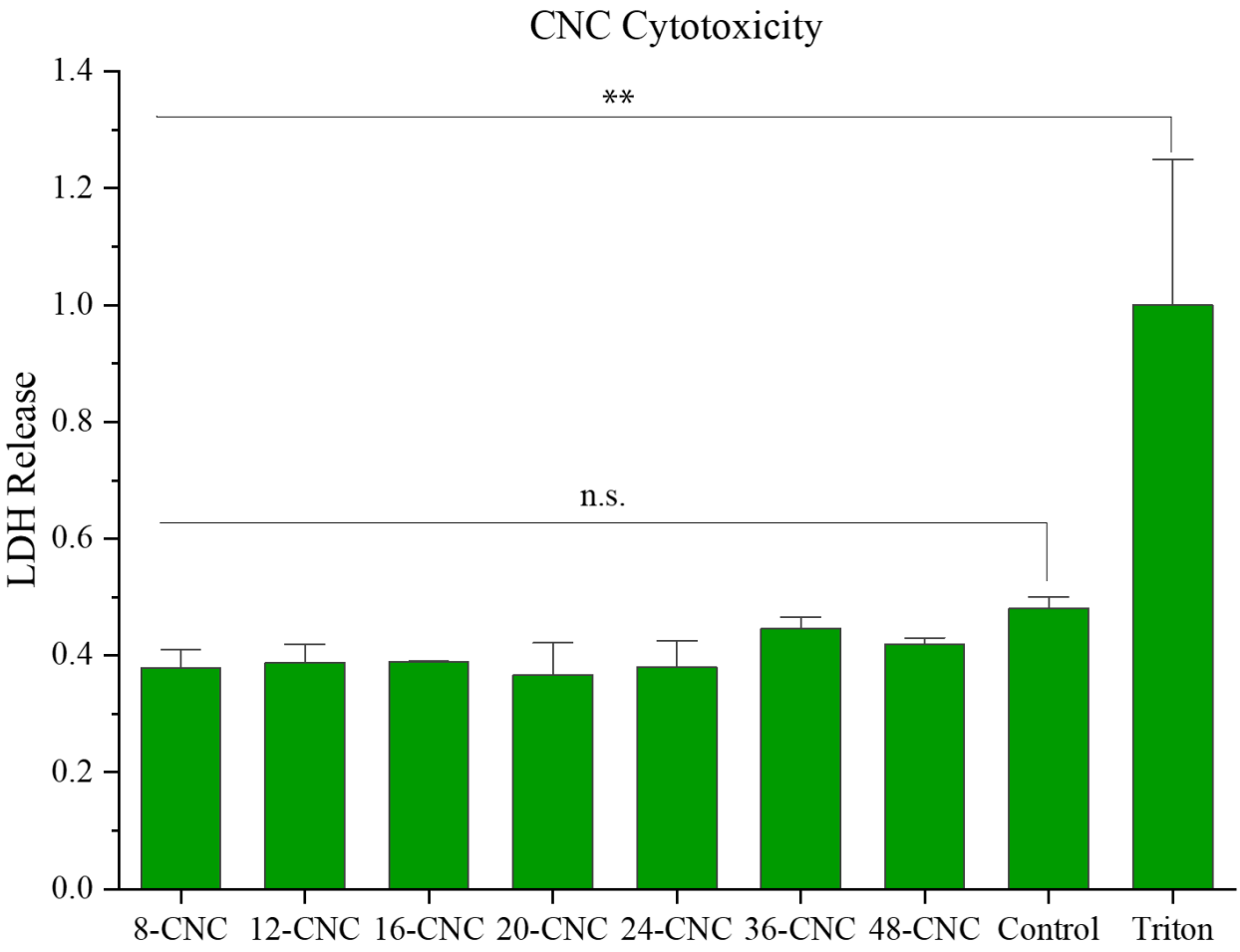

Figure 3.7*: Cytotoxicity studies of CNCs against ADSCs. The values are represented as absorbance values at 490 and 680 nm. Control and Triton represent spontaneous and maximum LDH release values. Statistical significances (p-value) were represented as ** $p \leq 0.001$.*

A hemocompatibility and cell viability study are recommended to determine if there are any differences between CNC reaction times and their effect on cells for biomedical applications.

3.5. Conclusion

APS swelling and oxidation shows that reaction time, ranging between 8 and 48 hours, has a significant impact on CNCs during the extraction process. Changes to the CNCs surface properties, colloidal stability, and size were confirmed by FTIR, long term aqueous suspension,

and AFM imaging, respectively. Surface charge also changed with reaction time, but there was no discernable pattern that we could see as to how the charge was impacted by reaction time. Mechanical analysis of 8-CNC, 24-CNC, and 48-CNC showed that there was no significant difference in the mechanical properties of CNCs with respect to reaction time, suggesting that reaction time does not impact the intrinsic mechanical properties of this material. Coating Ti with CNCs showed that reaction time does have an impact on the wettability of a surface. Lastly, it was found that APS oxidized CNCs are not cytotoxic towards ADSCs, and that reaction time has no impact on the nanoparticle's cytotoxicity. This study suggests that controlling reaction time could allow for more desirable and precise tuning of CNCs for various applications, particularly with medical implants. Future research would need to focus on attachment of the CNCs to Ti surfaces as well as hemocompatibility and cell viability, for desirable outcomes of Ti implants.

REFERENCES

(1) Delepierre, G.; Vanderfleet, O. M.; Niinivaara, E.; Zakani, B.; Cranston, E. D. Benchmarking Cellulose Nanocrystals Part II: New Industrially Produced Materials. *Langmuir* **2021**, *37* (28), 8393–8409. https://doi.org/10.1021/acs.langmuir.1c00550.

(2) Mali, P.; Sherje, A. P. Cellulose Nanocrystals: Fundamentals and Biomedical Applications. *Carbohydrate Polymers* **2022**, *275*, 118668. https://doi.org/10.1016/j.carbpol.2021.118668.

(3) Patil, T. V.; Patel, D. K.; Dutta, S. D.; Ganguly, K.; Santra, T. S.; Lim, K.-T. Nanocellulose, a Versatile Platform: From the Delivery of Active Molecules to Tissue Engineering Applications. *Bioactive Materials* **2022**, *9*, 566–589. https://doi.org/10.1016/j.bioactmat.2021.07.006.

(4) Punia Bangar, S.; Ilyas, R. A.; Chaudhary, N.; Dhull, S. B.; Chowdhury, A.; Lorenzo, J. M. Plant-Based Natural Fibers For Food Packaging: A Green Approach To The Reinforcement of Biopolymers. *J Polym Environ* **2023**, *31* (12), 5029–5049. https://doi.org/10.1007/s10924-023-02849-3.

(5) Novo, L. P.; Bras, J.; García, A.; Belgacem, N.; Curvelo, A. A. S. Subcritical Water: A Method for Green Production of Cellulose Nanocrystals. *ACS Sustainable Chem. Eng.* **2015**, *3* (11), 2839–2846. https://doi.org/10.1021/acssuschemeng.5b00762.

(6) Kang, X.; Kuga, S.; Wang, C.; Zhao, Y.; Wu, M.; Huang, Y. Green Preparation of Cellulose Nanocrystal and Its Application. *ACS Sustainable Chem. Eng.* **2018**, *6* (3), 2954–2960. https://doi.org/10.1021/acssuschemeng.7b02363.

(7) Man, Z.; Muhammad, N.; Sarwono, A.; Bustam, M. A.; Vignesh Kumar, M.; Rafiq, S. Preparation of Cellulose Nanocrystals Using an Ionic Liquid. *J Polym Environ* **2011**, *19* (3), 726–731. https://doi.org/10.1007/s10924-011-0323-3.

(8) Benhamou, K.; Dufresne, A.; Magnin, A.; Mortha, G.; Kaddami, H. Control of Size and Viscoelastic Properties of Nanofibrillated Cellulose from Palm Tree by Varying the TEMPO-Mediated Oxidation Time. *Carbohydrate Polymers* **2014**, *99*, 74–83. https://doi.org/10.1016/j.carbpol.2013.08.032.

(9) Bashar, M. M.; Zhu, H.; Yamamoto, S.; Mitsuishi, M. Highly Carboxylated and Crystalline Cellulose Nanocrystals from Jute Fiber by Facile Ammonium Persulfate Oxidation. *Cellulose* **2019**, *26* (6), 3671–3684. https://doi.org/10.1007/s10570-019-02363-7.

(10) Castro-Guerrero, C. F.; Gray, D. G. Chiral Nematic Phase Formation by Aqueous Suspensions of Cellulose Nanocrystals Prepared by Oxidation with Ammonium Persulfate. *Cellulose* **2014**, *21* (4), 2567–2577. https://doi.org/10.1007/s10570-014-0308-1.

(11) Culsum, N. T. U.; Melinda, C.; Leman, I.; Wibowo, A.; Budhi, Y. W. Isolation and Characterization of Cellulose Nanocrystals (CNCs) from Industrial Denim Waste Using Ammonium Persulfate. *Materials Today Communications* **2021**, *26*, 101817. https://doi.org/10.1016/j.mtcomm.2020.101817.

(12) Filipova, I.; Serra, F.; Tarrés, Q.; Mutjé, P.; Delgado-Aguilar, M. Oxidative Treatments for Cellulose Nanofibers Production: A Comparative Study between TEMPO-Mediated and Ammonium Persulfate Oxidation. *Cellulose* **2020**, *27* (18), 10671–10688. https://doi.org/10.1007/s10570-020-03089-7.

(13) Haunreiter, K. J.; Dichiara, A. B.; Gustafson, R. Nanocellulose by Ammonium Persulfate Oxidation: An Alternative to TEMPO-Mediated Oxidation. *ACS Sustainable Chem. Eng.* **2022**, *10* (12), 3882–3891. https://doi.org/10.1021/acssuschemeng.1c07814.
(14) Jiang, H.; Wu, Y.; Han, B.; Zhang, Y. Effect of Oxidation Time on the Properties of Cellulose Nanocrystals from Hybrid Poplar Residues Using the Ammonium Persulfate. *Carbohydrate Polymers* **2017**, *174*, 291–298. https://doi.org/10.1016/j.carbpol.2017.06.080.
(15) Khanjanzadeh, H.; Park, B.-D. Optimum Oxidation for Direct and Efficient Extraction of Carboxylated Cellulose Nanocrystals from Recycled MDF Fibers by Ammonium Persulfate. *Carbohydrate Polymers* **2021**, *251*, 117029. https://doi.org/10.1016/j.carbpol.2020.117029.
(16) Lam, E.; Leung, A. C. W.; Liu, Y.; Majid, E.; Hrapovic, S.; Male, K. B.; Luong, J. H. T. Green Strategy Guided by Raman Spectroscopy for the Synthesis of Ammonium Carboxylated Nanocrystalline Cellulose and the Recovery of Byproducts. *ACS Sustainable Chem. Eng.* **2013**, *1* (2), 278–283. https://doi.org/10.1021/sc3001367.
(17) Leung, A. C. W.; Hrapovic, S.; Lam, E.; Liu, Y.; Male, K. B.; Mahmoud, K. A.; Luong, J. H. T. Characteristics and Properties of Carboxylated Cellulose Nanocrystals Prepared from a Novel One-Step Procedure. *Small* **2011**, *7* (3), 302–305. https://doi.org/10.1002/smll.201001715.
(18) Liu, Y.; Liu, L.; Wang, K.; Zhang, H.; Yuan, Y.; Wei, H.; Wang, X.; Duan, Y.; Zhou, L.; Zhang, J. Modified Ammonium Persulfate Oxidations for Efficient Preparation of Carboxylated Cellulose Nanocrystals. *Carbohydrate Polymers* **2020**, *229*, 115572. https://doi.org/10.1016/j.carbpol.2019.115572.
(19) Madani, H.; Wibowo, A.; Judawisastra, H.; Nishiyama, N.; Budhi, Y. W. One-Step Extraction of Cellulose Nanocrystals from High Lignin Biomass through Ammonium Persulfate Oxidation Method. *Adv. Nat. Sci: Nanosci. Nanotechnol.* **2022**, *13* (1), 015007. https://doi.org/10.1088/2043-6262/ac549a.
(20) Marwanto, M.; Maulana, M. I.; Febrianto, F.; Wistara, N. J.; Nikmatin, S.; Masruchin, N.; Zaini, L. H.; Lee, S.-H.; Kim, N.-H. Effect of Oxidation Time on the Properties of Cellulose Nanocrystals Prepared from Balsa and Kapok Fibers Using Ammonium Persulfate. *Polymers* **2021**, *13* (11), 1894. https://doi.org/10.3390/polym13111894.
(21) Oun, A. A.; Rhim, J.-W. Isolation of Oxidized Nanocellulose from Rice Straw Using the Ammonium Persulfate Method. *Cellulose* **2018**, *25* (4), 2143–2149. https://doi.org/10.1007/s10570-018-1730-6.
(22) Wang, H.; Pudukudy, M.; Ni, Y.; Zhi, Y.; Zhang, H.; Wang, Z.; Jia, Q.; Shan, S. Synthesis of Nanocrystalline Cellulose via Ammonium Persulfate-Assisted Swelling Followed by Oxidation and Their Chiral Self-Assembly. *Cellulose* **2020**, *27* (2), 657–676. https://doi.org/10.1007/s10570-019-02789-z.
(23) Jiang, P.; Zhang, Y.; Hu, R.; Shi, B.; Zhang, L.; Huang, Q.; Yang, Y.; Tang, P.; Lin, C. Advanced Surface Engineering of Titanium Materials for Biomedical Applications: From Static Modification to Dynamic Responsive Regulation. *Bioactive Materials* **2023**, *27*, 15–57. https://doi.org/10.1016/j.bioactmat.2023.03.006.
(24) Vilaça, A.; Domingues, R. M. A.; Tiainen, H.; Mendes, B. B.; Barrantes, A.; Reis, R. L.; Gomes, M. E.; Gomez-Florit, M. Multifunctional Surfaces for Improving Soft Tissue Integration. *Adv. Healthcare Mater.* **2021**, *10* (8), 2001985. https://doi.org/10.1002/adhm.202001985.
(25) Asad, M.; Sana, M. Potential of Titanium Based Alloys in the Biomedical Sector and Their Surface Modification Techniques: A Review. *Proceedings of the Institution of*

Mechanical Engineers, Part C: Journal of Mechanical Engineering Science **2023**, 095440622311645. https://doi.org/10.1177/09544062231164506.
(26) Liu, Y.; Rath, B.; Tingart, M.; Eschweiler, J. Role of Implants Surface Modification in Osseointegration: A Systematic Review. *J Biomed Mater Res* **2020**, *108* (3), 470–484. https://doi.org/10.1002/jbm.a.36829.
(27) Akshaya, S.; Rowlo, P. K.; Dukle, A.; Nathanael, A. J. Antibacterial Coatings for Titanium Implants: Recent Trends and Future Perspectives. *Antibiotics* **2022**, *11* (12), 1719. https://doi.org/10.3390/antibiotics11121719.
(28) Im, J.-S.; Choi, H.; An, H.-W.; Kwon, T. Y.; Hong, M.-H. *Effects of Surface Treatment Method Forming New Nano/Micro Hierarchical Structures on Attachment and Proliferation of Osteoblast-like Cells*; preprint; Chemistry and Materials Science, 2023. https://doi.org/10.20944/preprints202307.0665.v1.
(29) Thu, M. K.; Kang, Y. S.; Kwak, J. M.; Jo, Y.-H.; Han, J.-S.; Yeo, I.-S. L. Comparison between Bone–Implant Interfaces of Microtopographically Modified Zirconia and Titanium Implants. *Sci Rep* **2023**, *13* (1), 11142. https://doi.org/10.1038/s41598-023-38432-y.
(30) Momeni, S.; Safder, M.; Khondoker, M. A. H.; Elias, A. L. Valorization of Hemp Hurds as Bio-Sourced Additives in PLA-Based Biocomposites. *Polymers* **2021**, *13* (21), 3786. https://doi.org/10.3390/polym13213786.
(31) Madruga, L. Y. C.; Sabino, R. M.; Santos, E. C. G.; Popat, K. C.; Balaban, R. de C.; Kipper, M. J. Carboxymethyl-Kappa-Carrageenan: A Study of Biocompatibility, Antioxidant and Antibacterial Activities. *International Journal of Biological Macromolecules* **2020**, *152*, 483–491. https://doi.org/10.1016/j.ijbiomac.2020.02.274.
(32) Abbasi Moud, A. Cellulose Nanocrystals Examined by Atomic Force Microscopy: Applications and Fundamentals. *ACS Food Sci. Technol.* **2022**, *2* (12), 1789–1818. https://doi.org/10.1021/acsfoodscitech.2c00289.
(33) Kassab, Z.; Abdellaoui, Y.; Salim, M. H.; Bouhfid, R.; Qaiss, A. E. K.; El Achaby, M. Micro- and Nano-Celluloses Derived from Hemp Stalks and Their Effect as Polymer Reinforcing Materials. *Carbohydrate Polymers* **2020**, *245*, 116506. https://doi.org/10.1016/j.carbpol.2020.116506.
(34) Klemm, D.; Heublein, B.; Fink, H.-P.; Bohn, A. Cellulose: Fascinating Biopolymer and Sustainable Raw Material. *Angew. Chem. Int. Ed.* **2005**, *44* (22), 3358–3393. https://doi.org/10.1002/anie.200460587.
(35) Brinchi, L.; Cotana, F.; Fortunati, E.; Kenny, J. M. Production of Nanocrystalline Cellulose from Lignocellulosic Biomass: Technology and Applications. *Carbohydrate Polymers* **2013**, *94* (1), 154–169. https://doi.org/10.1016/j.carbpol.2013.01.033.
(36) Trache, D.; Hussin, M. H.; Haafiz, M. K. M.; Thakur, V. K. Recent Progress in Cellulose Nanocrystals: Sources and Production. *Nanoscale* **2017**, *9* (5), 1763–1786. https://doi.org/10.1039/C6NR09494E.
(37) Hu, Y.; Tang, L.; Lu, Q.; Wang, S.; Chen, X.; Huang, B. Preparation of Cellulose Nanocrystals and Carboxylated Cellulose Nanocrystals from Borer Powder of Bamboo. *Cellulose* **2014**, *21* (3), 1611–1618. https://doi.org/10.1007/s10570-014-0236-0.
(38) Zhang, K.; Sun, P.; Liu, H.; Shang, S.; Song, J.; Wang, D. Extraction and Comparison of Carboxylated Cellulose Nanocrystals from Bleached Sugarcane Bagasse Pulp Using Two Different Oxidation Methods. *Carbohydrate Polymers* **2016**, *138*, 237–243. https://doi.org/10.1016/j.carbpol.2015.11.038.

(39) Khanjanzadeh, H.; Park, B.-D. Optimum Oxidation for Direct and Efficient Extraction of Carboxylated Cellulose Nanocrystals from Recycled MDF Fibers by Ammonium Persulfate. *Carbohydrate Polymers* **2021**, *251*, 117029. https://doi.org/10.1016/j.carbpol.2020.117029.
(40) El Achaby, M.; Kassab, Z.; Barakat, A.; Aboulkas, A. Alfa Fibers as Viable Sustainable Source for Cellulose Nanocrystals Extraction: Application for Improving the Tensile Properties of Biopolymer Nanocomposite Films. *Industrial Crops and Products* **2018**, *112*, 499–510. https://doi.org/10.1016/j.indcrop.2017.12.049.
(41) Wagner, R.; Raman, A.; Moon, R. Transverse Elasticity of Cellulose Nanocrystals Via Atomic Force Microscopy. Tenth International Conference on Wood & Biofiber Plastic Composites and Cellulose Nanocomposites Symposium, May 11-13, Madison, WI. Madison, WI: Forest Products Society, c2010. ISBN 978-1-892529-55-8.
(42) Zhao, T.; Jiang, L. Contact Angle Measurement of Natural Materials. *Colloids and Surfaces B: Biointerfaces* **2018**, *161*, 324–330. https://doi.org/10.1016/j.colsurfb.2017.10.056.
(43) Jung, J.; Choi, Y. J.; Lee, S. J.; Choi, Y.-S.; Douangdeuane, B.; Souliya, O.; Jeong, S.; Park, S.; Hwang, D. Y.; Seo, S. Promoting Effects of Titanium Implants Coated with *Dipterocarpus Tuberculatus* Extract on Osseointegration. *ACS Biomater. Sci. Eng.* **2022**, *8* (2), 847–858. https://doi.org/10.1021/acsbiomaterials.1c01220.
(44) Castro-Guerrero, C. F.; Gray, D. G. Chiral Nematic Phase Formation by Aqueous Suspensions of Cellulose Nanocrystals Prepared by Oxidation with Ammonium Persulfate. *Cellulose* **2014**, *21* (4), 2567–2577. https://doi.org/10.1007/s10570-014-0308-1.
(45) Zhang, Y.; Hosseinaei, O.; Wang, S.; Zhou, Z. Influence of Hemicellulose Extraction on Water Uptake Behavior of Wood Strands. *Wood and Fiber Science* **2011**, 244–250.
(46) TFS-AssetsLSGmanualsMAN0018500_CyQUANT-LDH-Cytotoxicity-Assay-Kit_PI.Pdf. https://assets.thermofisher.com/TFS-Assets%2FLSG%2Fmanuals%2FMAN0018500_CyQUANT-LDH-Cytotoxicity-Assay-Kit_PI.pdf (accessed 2024-07-23).

CHAPTER 4: CONCLUSIONS AND FUTURE WORK

4.1 Conclusions

The goal of this work was to extract CNCs from hemp biowaste using APS oxidation and analyze the physical properties of these particles. Furthermore, it was important to address if and how changing reaction time would impact CNCs physical, chemical, morphological, and mechanical properties. Extraction of CNCs was clearly demonstrated by two separate projects.

One-step APS oxidation was used to extract CNCs from hemp biowaste. CNCs were separated into two groups: one groups only underwent washing using distilled water and a second group had an additional cleaning step to completely remove all non-cellulose materials. Differences between groups were seen using chemical analysis techniques, indicating the effectiveness of using an additional cleaning step during the CNC cleaning process. However, there were no differences in the size of the nanoparticles, suggesting that the additional cleaning step purely removed remaining unwanted materials after extraction. Mechanical analysis performed on CNCs using Force/Distance spectroscopy showed that the additional purification step also does not affect CNCs Young's modulus. Furthermore, it was found that the CNCs Young's modulus was not impacted whether individual CNCs were distinctly separated from one another or agglomerated in large groups.

A modified one-step APS oxidation technique was used that greatly reduced the reaction time required to extract CNCs from hemp biowaste, compared to the first study. Results demonstrated that adjusting reaction time, while keeping all other reaction conditions the same, had a direct impact on final product. As reaction time increased, the size of CNCs decreased and became more uniform and the amount of final product also decreased. Changing reaction time

impacted some of the surface properties of CNCs and had an effect on Ti surfaces hydrophilicity. Reaction time did not, however, have a statistically significant impact on surface charge, cytotoxicity, or Young's modulus of the final product. CNCs at all reaction times were found to be cytocompatible with ADSCs.

The overall results of the experiments contained in this document advocate the use of hemp biowaste as a source of CNC extraction via APS oxidation as an environmentally friendly method. Use of hemp biowaste and APS can create a circular economy and decrease environmental hazardous waste. The results suggest that certain CNC properties, such as size and final product volume, can be adjusted by varying reaction parameters, but properties, such as Young's modulus, are strictly determined by the source material.

4.2 Future Work

4.2.1 CNC binding to Titanium

Titanium is commonly used for medical implants[1]. CNCs are natural polymers that could be used as biomaterials as a potentially valuable method for modifying Ti surfaces on implants to increase attachment and longevity of the device in a body[2]. It was observed that coating Ti with CNCs caused a significant increase in the wettability of its surface. Future work could be directed at optimizing binding of CNCs to Ti. This would result in better attachment of CNCs on the surface and prevent unwanted loss during sterilization processes prior to implantation. Furthermore, this would potentially add micro- and nano-scale changes to the surface topography, potentially aiding in cellular attachment as well as overall integration of Ti implants[3].

4.2.2 CNC surface modification

CNCs have highly modifiable surfaces. These surfaces can undergo modification via the removal or addition of chemicals, molecules, polymers, and proteins using various reaction[4,5]. This was seen by removal of lignin and hemicellulose during extraction and the addition of carboxyl groups. Future research could be directed at modifying the surface of CNCs either prior to or after application on Ti surfaces. Selectively modifying CNCs attached to Ti surfaces could potentially increase chemotaxis, cytocompatibility, hemocompatibility, and cellular attachment to a Ti implant surface.

4.2.3 Electrospinning CNCs

Electrospinning is an additive manufacturing application that can be used to create many different kinds of things. Electrospinning nanofibers and microfibers has been utilized for the application of bandages and films in biomedical applications[6]. CNCs have been shown to increase films and nanocomposite mechanical strength by being used as a natural polymer[7]. It would be of interest to include these nanoparticles into electrospun fibers to increase mechanical properties. Also, the use of CNCs to replace synthetic polymers could increase electrospun fibers biocompatibility for use in various wound applications. Furthermore, it has been shown that CNCs impact diffusion of molecules when they are incorporated into various medical products[8,9]. Therefore, it would be interesting to research how CNCs incorporated into electrospun fibers with drugs would impact their controlled release at wound sites.

REFERENCES

(1) Asad, M.; Sana, M. Potential of Titanium Based Alloys in the Biomedical Sector and Their Surface Modification Techniques: A Review. *Proceedings of the Institution of Mechanical Engineers, Part C: Journal of Mechanical Engineering Science* **2023**, 095440622311645. https://doi.org/10.1177/09544062231164506.

(2) Kulkarni, M.; Mazare, A.; Schmuki, P.; Iglič, A. Biomaterial Surface Modification of Titanium and Titanium Alloys for Medical Applications.

(3) Souza, J. C. M.; Sordi, M. B.; Kanazawa, M.; Ravindran, S.; Henriques, B.; Silva, F. S.; Aparicio, C.; Cooper, L. F. Nano-Scale Modification of Titanium Implant Surfaces to Enhance Osseointegration. *Acta Biomaterialia* **2019**, *94*, 112–131. https://doi.org/10.1016/j.actbio.2019.05.045.

(4) Natterodt, J. C.; Petri-Fink, A.; Weder, C.; Zoppe, J. O. Cellulose Nanocrystals: Surface Modification, Applications and Opportunities at Interfaces. *CHIMIA* **2017**, *71* (6), 376–376. https://doi.org/10.2533/chimia.2017.376.

(5) Eyley, S.; Thielemans, W. Surface Modification of Cellulose Nanocrystals. *Nanoscale* **2014**, *6* (14), 7764–7779. https://doi.org/10.1039/C4NR01756K.

(6) Sun, Y.; Heacock, J.; Chen, C.; Qiu, K.; Zou, L.; Liu, J.; Li, Y. V. Incorporation of Gentamicin-Encapsulated Poly(Lactic-Co-Glycolic Acid) Nanoparticles into Polyurethane/Poly(Ethylene Oxide) Nanofiber Scaffolds for Biomedical Applications. *ACS Appl. Nano Mater.* **2023**, *6* (17), 16096–16105. https://doi.org/10.1021/acsanm.3c03549.

(7) Shi, Q.; Zhou, C.; Yue, Y.; Guo, W.; Wu, Y.; Wu, Q. Mechanical Properties and in Vitro Degradation of Electrospun Bio-Nanocomposite Mats from PLA and Cellulose Nanocrystals. *Carbohydrate Polymers* **2012**, *90* (1), 301–308. https://doi.org/10.1016/j.carbpol.2012.05.042.

(8) Haque, P.; Tabassum, M. Hydroxyapatite and Cellulose Nanocrystals Loaded Gelatin-Chitosan Based Electrospun Nanofibrous Mats for Rapid Wound Healing. Rochester, NY May 22, 2023. https://doi.org/10.2139/ssrn.4455528.

(9) Hivechi, A.; Bahrami, S. H.; Siegel, R. A. Drug Release and Biodegradability of Electrospun Cellulose Nanocrystal Reinforced Polycaprolactone. *Materials Science and Engineering: C* **2019**, *94*, 929–937. https://doi.org/10.1016/j.msec.2018.10.037.